SLAC-PUB-15442

Prepared for submission to JCAP

Unbound Particles in Dark Matter Halos

Peter S. Behroozi,[a] **Abraham Loeb,**[b] **Risa H. Wechsler**[a]

[a]Kavli Institute for Particle Astrophysics and Cosmology; Physics Department, Stanford University, and SLAC National Accelerator Laboratory,
2575 Sand Hill Road, Menlo Park, CA, USA
[b]Department of Astronomy, Harvard University,
60 Garden St, Cambridge, MA, USA

E-mail: behroozi@stanford.edu

Abstract. We study the properties of unbound dark matter particles, defined as having sufficient kinetic energy to escape the boundary of their parent halos. We find that the mass fraction of unbound particles increases strongly towards the edges of halos and in denser environments. Mergers are the largest source of unbound particles; however, major mergers are not especially more efficient than minor mergers in this regard. Because unbound dark matter particles can leave halos more easily than their baryonic counterparts, we also find that standard ΛCDM cosmology predicts a redshift-dependent boost for the baryon fraction in massive clusters which reaches as high as an extra ~ 20 percent at $z = 0$ compared to the universal value. Our findings have relevance for dark matter detection experiments, precision calibrations of the halo mass function, the use of baryon fractions to constrain dark energy, and searches for intergalactic supernovae.

Keywords: dark matter, N-body simulations, cosmology:theory

Published in arXiv:1208.0334.

Work supported in part by US Department of Energy under contract DE-AC02-76SF00515.

Contents

1 Introduction

Unbound particles represent a small fraction of the mass in dark matter halos [1], but they carry the highest energies in the dark matter velocity distribution function. This property means that unbound particles can have unexpected importance for experimental and observational interpretations, including those for dark matter detection experiments, precision cosmology surveys, baryon fraction measurements, and searches for intergalactic supernovae.

Direct detection experiments are sensitive to the velocity distribution of dark matter. This has led to many studies of the expected phase-space distribution of dark matter particles [2–10]. Although conclusive results have yet to emerge from the experiments themselves, many groups have recently started to probe the range of collisional cross-sections and particle masses most favored by theoretical physicists [11–15]. With possible discovery on the horizon, it is important to better constrain the velocity distribution of the Milky Way, as well as to better understand the sources of halo-halo variation in the high-energy (e.g., unbound) dark matter fraction.

Another reason for studying unbound particles comes from observational surveys which aim to place precision constraints on cosmology (e.g., BOSS, DES, BigBOSS, Pan-STARRS, eRosita, Herschel, Planck, JWST, and LSST; [16–24]). In order to fully realize their statistical power, these surveys depend on precision calibrations of the halo mass function to 1% or

better accuracy [25, 26]. Traditionally, halo mass functions have been calibrated from gravity-only ("dark matter") simulations [27–31]. These calibrations are expected to be inaccurate within several galaxy scale lengths due to baryonic feedback effects [32, 33], but there is also another bias at large scales (e.g., at the virial radius) due to the effects of unbound dark matter particles.

Specifically, high-energy dark matter can freely enter and leave halos, but high-energy baryons will collide with the gas already present in the halo and remain behind. Dark matter simulations capture the first effect but not the second, leading to an underestimate of both the halo density at large scales and the halo mass. This effect also suggests that the local baryon fraction should increase beyond the cosmic average on the outskirts of clusters. In fact, this has already been detected in simulations [34] and in observations [35]. However, because clumpiness in the intracluster medium can also produce a similar observational signature, proper interpretation of the result in [35] requires exploration of the relative contribution from both effects.

Observations of intergalactic supernovae [36–38] also relate to unbound particles, especially observations of supernovae traveling at high speeds [39]. Such high-velocity supernovae might either come from the intracluster stellar population [38, 40], from merging events [41, 42], or from hypervelocity stars ejected from the central galaxy [43]. Since stars are effectively collisionless and so have similar dynamics to dark matter, one can place an effective upper limit on the expected high-velocity supernova rate from stars pre-existing in the intracluster stellar population by analyzing the unbound fraction of the dark matter velocity distribution as a function of radius.

Finally, we note that the unbound fraction of dark matter in halos involves an important definitional issue. In the analysis of dark matter simulations to recover dark matter halos, many halo finders remove unbound particles (e.g., [1, 44–47]). The usual justification for this choice is that unbound particles will quickly leave the system, representing a transient population which will not contribute to the long-term mass of the halo. However, some halo finders do not remove unbound particles (e.g., [28, 48]), so it is interesting to consider how much the observed discrepancies between halo finders (see, e.g., [49]) depend on this choice. Moreover, the assumed definition for bound particles traditionally uses the Newtonian escape condition (kinetic energy greater than the absolute value of the Newtonian potential energy), which has not been appropriately verified in an expanding cosmology.

These reasons have motivated us to conduct a comprehensive study of the population of unbound particles in dark matter halos. In §2, we discuss the dark matter simulation we employ as well as the halo finder and conventions used for calculating kinetic and potential energies. We present the main results for the population of unbound particles in §3 and discuss how these results impact the science considerations above in §4. Finally, we summarize our conclusions in §5. Throughout this work, we adopt a flat, ΛCDM cosmology with main parameters $\Omega_b = 0.04$, $\Omega_M = 0.25$, $\Omega_\Lambda = 0.75$, and $h = 0.7$; this is similar to the WMAP7 best-fit cosmology constraints [50].

2 Methods and Conventions

2.1 Simulation

We make use of the *Consuelo* simulation from the Large Suite of Dark Matter Simulations (McBride et al, in preparation).[1] Consuelo covers a large volume (420 h^{-1} Mpc on a side)

[1] LasDamas Project, `http://lss.phy.vanderbilt.edu/lasdamas/`

with ∼2.7 billion particles (1400^3), corresponding to a particle mass resolution of 2.7×10^9 $M_\odot$. Its large size and resolution make it ideal for particle studies from Milky Way-sized halos ($10^{12} M_\odot$, 400 particles) to the largest clusters ($10^{15} M_\odot$, 400,000 particles). The simulation was performed using GADGET-2 [51] with collisionless dark matter only, with a force softening length of 8 h^{-1} kpc. The assumed simulation conditions were a flat, ΛCDM cosmology ($\Omega_M = 0.25$, $\Omega_\Lambda = 0.75$, $h = 0.7$, $\sigma_8 = 0.8$, and $n_s = 1.0$), which is similar to the WMAP7 best-fit cosmology [50]. From this simulation, 100 snapshots were saved from $a = 0.075$ to $a = 1.0$, spaced at uniform logarithmic intervals in scale factor.

In a few cases where resolution tests are necessary, we make use of the *Esmeralda* simulation, also from the LasDamas Project. This simulation was run with identical parameters and software as the Consuelo simulation, with the exception of its box size (640 h^{-1} Mpc, particle count (1250^3), mass resolution (1.33×10^{10} $M_\odot$, and force resolution (15 h^{-1} kpc).

2.2 Halo Finding and Properties

Halo finding was performed using the ROCKSTAR algorithm, which is a phase-space temporal (7D) halo finder designed for high consistency and accuracy of halo properties [1, 52]. The ROCKSTAR halo finder locates peaks in the particle phase-space density distribution using a locally adaptive phase-space metric. A seed halo is placed at the location of each peak, and particles are assigned to the closest seed halo in phase space (see [1] for full details). Particle potentials are computed using a tree method (see §2.3), and unbound particles are removed before calculating halo properties (spherical overdensities, radii, spins, etc.).

In this analysis, we consider host halos only (i.e., halos whose centers are not within the radius of more massive halos). This is because satellite halos (i.e., non-host halos) are almost always *defined* as a collection of self-bound particles within a larger halo: as such, they have no unbound particles to analyze. For cases where host / satellite halo relationships are ambiguous (such as in major mergers), ROCKSTAR uses the host/satellite relationship at the previous snapshot if available.

We restrict our analysis to halos with more than 400 particles, which have been shown to have robustly measurable properties when compared to higher-resolution resimulations [53]. Halo virial masses and virial radii are defined according to the spherical overdensity criterion of [54]; if a halo includes satellite halos within its virial radius, those are considered to contribute towards its virial mass.

2.3 Kinetic and Potential Energy Calculation

An individual particle is considered to be bound to a halo if the sum of its physical kinetic energy and its potential energy (relative to all other particle positions within the halo radius) is negative. Calculating particle kinetic energies is straightforward ($\frac{1}{2}v^2$ per unit mass), where v is the physical velocity of the particle relative to the halo bulk velocity. However, the calculation of potential energies in expanding cosmologies poses normalization issues—the usual practice of setting the potential to zero at infinity is not well-defined. The standard method for bound/unbound classification is to ignore these issues and compute particle potentials in a Newtonian metric, so that the potential ϕ of a point mass M (i.e., the Green's function) is

$$\phi(r) = -\frac{GM}{r} \tag{2.1}$$

This is the approach taken by, for example, [44–47] and [1]. For completeness, we consider both this traditional definition as well as alternate definitions in §3.1, where $\phi = 0$ for a

chosen finite radius R_0; this latter case corresponds to substituting the following Green's function:

$$\phi(r) = -\frac{GM}{r} + \frac{GM}{R_0}. \tag{2.2}$$

To calculate particle gravitational potentials, we use a modified Barnes-Hut algorithm [55], as detailed in [1]. This method is nearly as accurate as a direct N^2 potential calculation [1]; however, as it is a tree-based ($\mathcal{O}(N \log N)$) algorithm, it is much faster.

In our analysis, we consider a range of particle binding energies, so it is helpful to define the boundedness b, of a particle as

$$b = \frac{|PE| - KE}{|PE|} \tag{2.3}$$

where KE and PE are the kinetic and potential energies, respectively, of the particle. A value of $b = 1$ indicates that the particle has no kinetic energy (is completely bound); a value of $b = 0$ indicates that the particle is marginally unbound (kinetic energy equals negative potential energy).

From the virial theorem, one might expect that the average value of b within the virial radius of a halo should be $b = 0.5$. However, this is not the case for several reasons: the force law in an expanding cosmology is not a simple r^{-2} law (see Eq. (3.2)), not all particle orbits stay within the virial radius (see §3.4), and the "virial" radius used here is set via a fixed overdensity threshold but cosmological halos are consistently perturbed away from virialization by mergers. The combination of these factors makes the average value of b within the virial radius of the halos in this study about 0.6 to 0.7.

3 Results

We first discuss the statistics of the fraction of unbound particles in halos and explore the variation in this fraction with respect to radius, redshift, halo mass, potential definition, halo definition and environment in §3.1. Next, we discuss the energy requirements for a particle to escape to infinity in an expanding cosmology and compare these to Newtonian energy requirements in §3.2. We then consider the particles which actually escape from halos and discuss their origins, orbits, and likely future trajectories in §3.3 and §3.4. Finally, we discuss the effects of unbound particles on the baryon fraction of clusters in §3.5.

3.1 Fractional Occurrence of Unbound and Nearly Unbound Particles in Halos

3.1.1 Average, Radial, and Redshift Dependence

The definition of an unbound particle is nominally unambiguous: a particle with enough kinetic energy to leave its surrounding potential well. However, there can be many different choices for what the appropriate potential well should be. Two categories of high-energy particles which have particular physical importance are those which can leave the virial radius of the halo ("unbound" with $\phi(R_{\rm vir}) = 0$) and those which can leave the halo and never come back ("unbound" with $\phi(\infty) = 0$, as in Eq. (2.1)). We consider both categories of particles here, but we note that most dependencies (on redshift, environment, etc.) are very similar for both, so we only show figures for both categories when substantial differences occur. In the text and figures, we always specify which potential definition ($\phi(R_{\rm vir}) = 0$ or $\phi(\infty) = 0$) is being discussed.

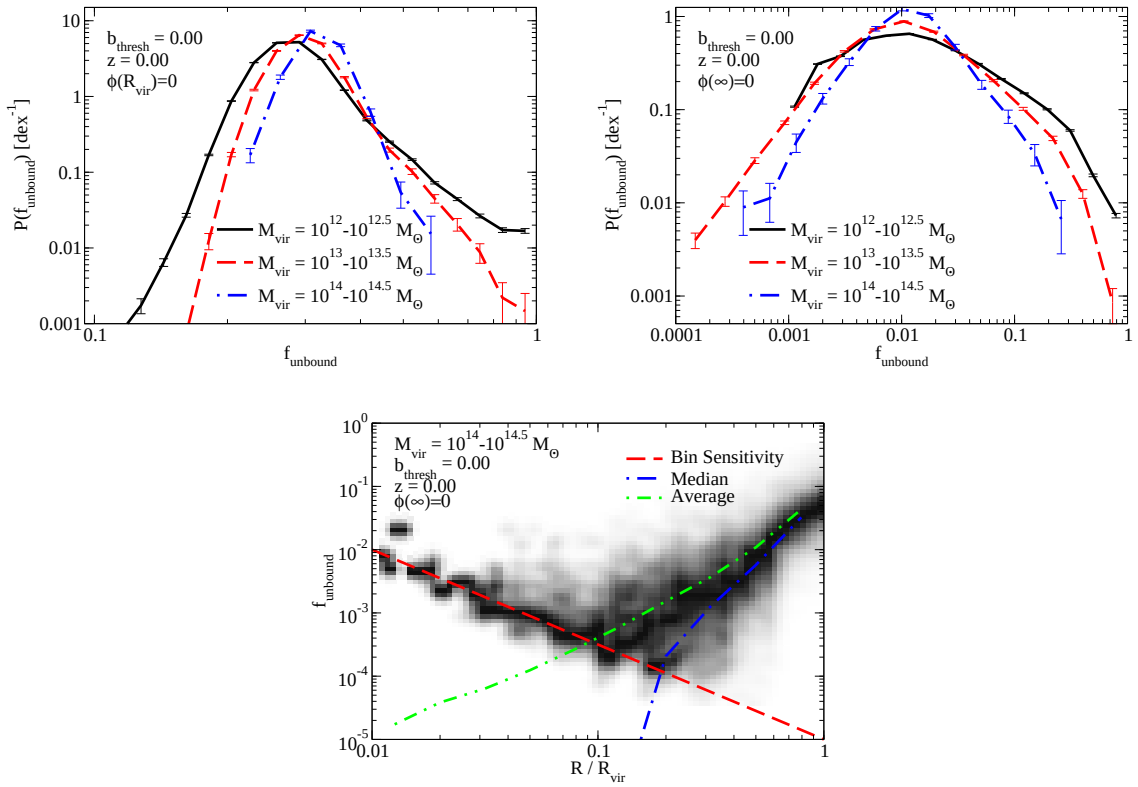

Figure 1. There are two main definitions of "unbound"—the first is the ability to escape the host halo's virial radius, and the second is the ability to escape to infinity. The **top-left panel** shows the probability distribution of unbound mass fractions according to the first definition ($\phi(R_{\rm vir}) = 0$) as a function of halo mass at $z = 0$; this averages around 30%. The **top-right panel** shows the probability distribution of the unbound fraction which can escape to infinity ($\phi(\infty) = 0$) as a function of halo mass at $z = 0$, which averages only about 2-3%. The **bottom panel** shows the conditional density distribution of the latter unbound particle fraction ($\phi(\infty) = 0$) as a function of radius in massive ($10^{14} M_\odot < M_{\rm vir} < 10^{14.5} M_\odot$) halos at $z = 0$. The **red dashed line** shows the limit of one particle per radial bin; effectively, the individual halo sensitivity limit. Because the unbound fraction as a whole passes below this limit at small radii, the median unbound fraction (**blue dot-dashed line**) rapidly drops to zero from the floor effect. On the other hand, the average unbound fraction (**green double dot-dashed line**) follows the trend established at higher radii down to a small fraction of the virial radius.

One caveat with this analysis is that, as explained in §3.2, the energy threshold for escape to infinity in an expanding cosmology can vary by ±10% at $z = 0$ (depending on halo mass) as compared to the Newtonian escape threshold. To enable better interpretations of other results, especially in terms of the "bound" masses reported by halo finders, we keep to the traditional Newtonian energy thresholds. In practice, a particle unbound with respect to the standard Newtonian escape thresholds for $z < 1$ will always leave the halo radius and will, at minimum, not return for a large number of dynamical times.

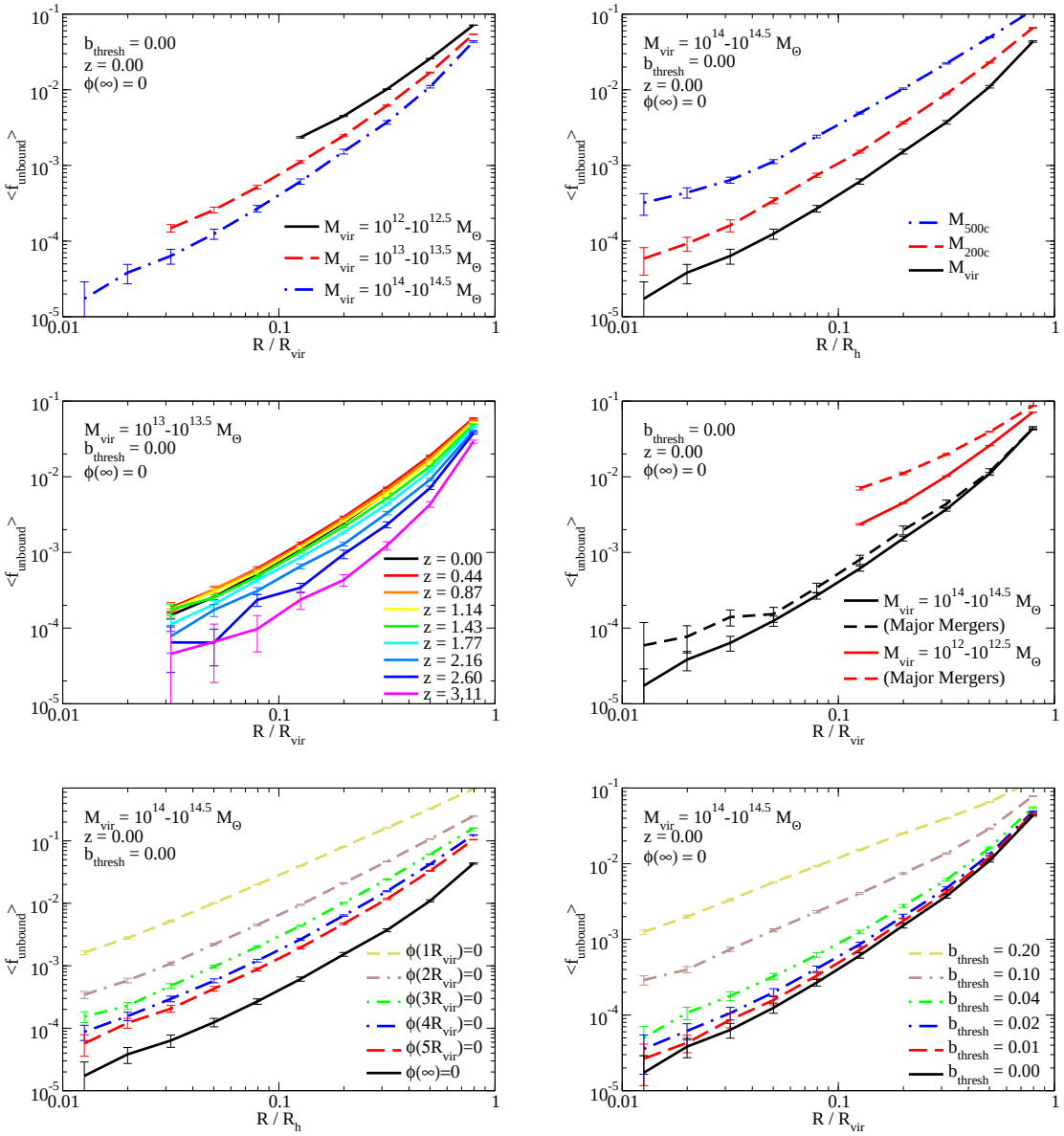

Figure 2. **Top-left panel**: The average unbound fraction as a function of mass and radius; smaller halos have more unbound particles. For this and other panels, limited resolution prevents calculating unbound fractions within 16 h^{-1} kpc of halo centers. **Top-right panel**: The unbound fraction as a function of radius for alternate halo definitions (i.e., spherical regions enclosing 200 and 500 times the critical density). Approximately four times as many particles are unbound if R_{500c} is used as the halo radius instead of R_{vir}. Note that the potential ϕ is calculated only using particles within the halo radius; thus, a given particle in the halo will appear less bound if a higher overdensity definition is used. **Middle-left panel**: The unbound fraction as a function of radius and redshift for $10^{13} - 10^{13.5} M_{\odot}$ halos. The unbound fraction appears unchanged to $z = 1$, but drops off significantly above that redshift. **Middle-right panel**: The unbound fraction for all halos as compared to halos undergoing major mergers. Halos in major mergers have surprisingly few extra unbound particles, on average. **Bottom-left panel**: The average unbound fraction as a function of the potential zero-point definition (i.e., the radius beyond which "unbound" particles can travel). Most particles have enough kinetic energy to leave the virial radius of the halo, but less than half as many have enough kinetic energy to make it to twice the virial radius. **Bottom-right panel**: The fraction of marginally bound particles as a fraction of the boundedness threshold $b_{\rm thresh}$. For each particle, the boundedness b is calculated as its kinetic plus potential energies divided by its potential energy (Eq. (2.3)). A value of $b < 0$ implies that the particle is unbound; larger values of b (up to $b = 1$) imply that the particle is more and more bound. In this panel, it is clear that the fraction of marginally bound particles is significantly more than the fraction of unbound particles (e.g., up to twice as much for particles which are within 10% of being unbound); however, it remains extremely difficult to unbind particles from the central regions of halos. Error bars for all panels are calculated using jackknife statistics.

Individual host halos can have a wide variety of unbound particle fractions at $z = 0$, as shown in the top panels of figure 1. On average, about 30% of particles in halos at $z = 0$ can escape the halos' virial radii ($\phi(R_{\rm vir}) = 0$), whereas only 2-3% can escape to infinity ($\phi(\infty) = 0$). The width of the distribution in both cases is substantially wider for Milky-Way-sized halos ($10^{12} M_\odot < M_{\rm vir} < 10^{12.5} M_\odot$) as compared to massive halos ($10^{14} M_\odot < M_{\rm vir} < 10^{14.5} M_\odot$). This is especially pronounced for the $\phi(\infty) = 0$ case, where the scatter across halos doubles from 0.3 dex in massive halos to 0.6 dex in Milky-Way-sized ones.[2] We have verified that these probability distributions are identical for our lower-resolution simulation. Smaller halos live in a greater diversity of environments; by comparison, massive halos will not be found in very isolated environments, nor will they be found near relatively much larger halos, which contributes to the larger scatter seen. We address the environmental dependence explicitly in §3.1.2.

We note that some halos in the top panels of Fig. 1 can have very high unbound fractions, approaching 100%. These high unbound fractions occur when a smaller halo partially overlaps with one or more larger ones. Specifically, all particles within the virial radius of the smaller halo will be counted towards its mass, even though those particles may also be within the virial radii of the larger halos nearby. These shared particles will have higher velocity dispersion from their association with the larger halos, which can lead to very large unbound fractions for the smaller halo.

The bottom panel in figure 1 shows the spread in unbound fractions ($\phi(\infty) = 0$) as a function of radius for massive halos at $z = 0$. The significant scatter seen in figure 1 remains at all radii. However, at small radii ($< 0.1 R_{\rm vir}$), the average unbound fraction is so low that most halos will have less than a single unbound particle per radial bin. As a consequence, the median unbound fraction across halos significantly underestimates the overall trend at small radii. For that reason, we express radial unbound fractions in terms of the average across all halos, which better follows the trend of unbound fractions established at larger radii.

The average radial profile of the unbound fraction (i.e., the ratio of unbound to total particles in radial bins) is shown in figure 2, in most cases for $\phi(\infty) = 0$. In all cases, the unbound fraction increases as a strong power-law with radius; the logarithmic slope ranges between 1.5 and 2, steepening towards the outer regions of the halos in question. For a NFW [56] halo density profile, this would imply that the physical density of unbound particles peaks between one and two times the scale radius.

The top-left panel in figure 2 shows the mass dependence of the radial dependence of the average unbound fraction. As in the top panel of figure 1, smaller halos have larger unbound fractions across all radii; at large radii the absolute difference is larger than at small radii. For smaller halos in this panel, the radial dependence is truncated at twice the force resolution of the simulation (16 h^{-1} kpc), as the gravitational accuracy of the simulation degrades rapidly below that radius.

The top-right panel in figure 2 shows how the unbound fraction ($\phi(\infty) = 0$) changes based on the halo mass definition. If the [54] spherical overdensity threshold is replaced by another common but higher density definition for massive halos (e.g., 200 or 500 times the critical density), then significantly more particles are unbound if the potential is calculated only within the halo radius. This is exactly as might be expected: the higher density definitions amount to truncating the halo at a smaller radius, reducing the total mass enclosed but without reducing the velocity dispersion. The top panel in figure 3 shows for comparison

[2] Smaller halos have fewer particles, which introduces a binomial sampling scatter when calculating unbound fractions. However, for the smallest halos we consider ($10^{12} M_\odot$), this scatter is a negligible 0.1 dex.

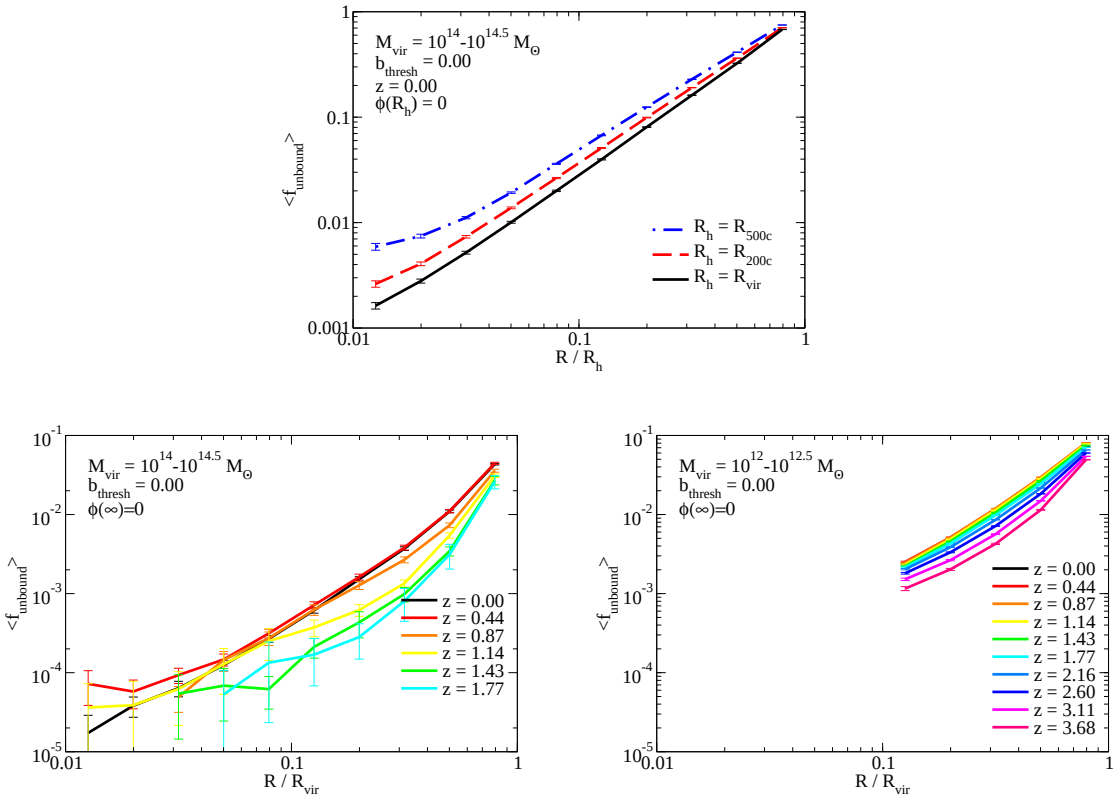

Figure 3. Supplemental panels for figure 2. The **top** panel shows how the unbound fraction depends on the halo mass definition if the potential is defined such that $\phi(R_h) = 0$, rather than $\phi(\infty) = 0$. This is equivalent to the fraction of particles which would be expected to have orbits outside the halo radius. As compared to the figure for the $\phi(\infty) = 0$ case in figure 2, the different halo definitions result in much more similar unbound fractions. The **bottom** panels show the evolution of the unbound fraction as a function of radius and redshift for two more mass bins (left panel: $10^{14} - 10^{14.5} M_\odot$; right panel: $10^{12} M_\odot - 10^{12.5} M_\odot$) than shown in figure 2. As with the analogous panel in figure 2, very little evolution in the unbound fraction is seen to $z \sim 1$. However, the exact redshift where the unbound fraction begins to change does have a slight mass dependence. This may be related to the fact that halos which are the dominant sources of mass in their nearby environment have lower unbound fractions.

the fraction of particles which can pass beyond the halo radius ($\phi(R_h) = 0$) for the various mass definitions, which is much more stable.

The middle-left panel in figure 2 shows the redshift dependence of the radial unbound fraction, which has apparently no evolution out to $z = 1$. At higher redshifts, however, the unbound fraction falls substantially. This trend is preserved across all the mass ranges we consider, as shown in the bottom two panels of figure 3.

The middle-right panel in figure 2 shows how the unbound fraction changes if only halos undergoing major mergers are selected. Specifically, a halo is considered to be undergoing a major merger if it contains a satellite halo with $v_{\rm max,sat} > 0.6 v_{\rm max,host}$, where $v_{\rm max}$ is the maximum circular velocity, corresponding approximately to an infalling mass ratio of 0.3:1. This panel shows that, for massive halos, the presence of a major merger has very little impact on the unbound fraction. However, for less-massive halos (e.g., $10^{12} M_\odot < M_{\rm vir} < 10^{12.5} M_\odot$),

a major merger can increase the unbound fraction somewhat more (by 1–2% overall). At first glance, it may appear surprising that halos undergoing major mergers do not have substantially more unbound particles. However, recalling the definition of the halo mass as a spherical overdensity, the mass in an incoming major merger gets added to that of the host as it crosses the virial radius. Hence, while the incoming particles may have been unbound relative to the potential of the original halo, they are mostly bound relative to the *combined* potential of the incoming and original particles within the virial radius. This effect is explicitly shown in §3.1.2.

The bottom-left panel in figure 2 shows how the unbound fraction would change if the zero-point of the Newtonian potential were set at a location other than infinity (see Eq. (2.2)). Note that if $\phi(R_0) = 0$ for a specific choice of R_0, then the unbound particles ($b < 0$) for this choice of ϕ are exactly those which have enough kinetic energy that their trajectories can reach R_0. For larger values of R_0, the orbital time will increase. As a rough guide, the free-fall time of a particle towards a point mass will be $\sqrt{2R^3(GM)^{-1}}$, so a particle on a radial orbit would spend a time

$$t_{\rm out} = \frac{4}{\sqrt{2GM_{\rm vir}}}\left(R_0^{\frac{3}{2}} - R_{\rm vir}^{\frac{3}{2}}\right) \tag{3.1}$$

outside of the halo. This can be very large even for relatively close distances; particles with enough energy to reach $1.1R_{\rm vir}$ will spend about 1Gyr outside the halo, and those with enough energy to reach $2R_{\rm vir}$ will spend at least 10Gyr outside of the halo. Thus, perhaps 20-25% of the particles in halos at $z = 0$ have enough energy to take very long trips outside of the virial radius; this is similar to the fraction of particles (25%) which take extended trips out of Friends-of-Friends halos [57] .

Finally, the bottom-right panel in figure 2 shows the radial dependence of marginally bound particles. A range of boundedness thresholds (b, see Eq. (2.3)) are considered, from $b < 0.01$ (within 1% or less of being unbound) to $b < 0.2$ (within 20% or less of being unbound). The results in §3.2.2, which account for the effects of halo mass accretion and the expansion of the universe, suggest that the appropriate energy threshold for a particle to escape to infinity at $z = 0$ for halos in this mass range (10^{14} to $10^{14.5} M_\odot$) is about $b \sim 0.05$ at $R = 0$ and $b \sim 0.18$ at the virial radius. Thus, about 10% of the particles close to the virial radius have enough energy to leave the halo and never come back.

To summarize the most important trends, the unbound fraction is a strong function of radius. Regardless of definition, the unbound fraction on galaxy scales (within $0.05R_{\rm vir}$) is below 1%, whereas it can reach 10-100% (depending on definition) at the halo radius. Major mergers, lower halo masses, and lower redshifts all correlate with increased unbound fractions, but these effects are comparatively subdominant.

3.1.2 Environmental Dependence

One way to explain the mass dependence of unbound fractions in the top panel of figure 1, is through an environmental dependence of the unbound fraction. There are several ways of quantifying the local environment; one common method is to use the distance to the nearest larger halo. As shown in the top-left panel of figure 4, the unbound fraction for Milky Way-sized halos ($\phi(\infty) = 0$) has a very clear dependence on this measure of environment, with the unbound fraction increasing by a factor of 30 over the range of 1-10 Mpc. This dependence is even clearer if the distance to the larger halo is scaled by the larger halo's virial radius (figure 4, bottom-left panel), strongly suggesting that tidal forces and/or an increase in

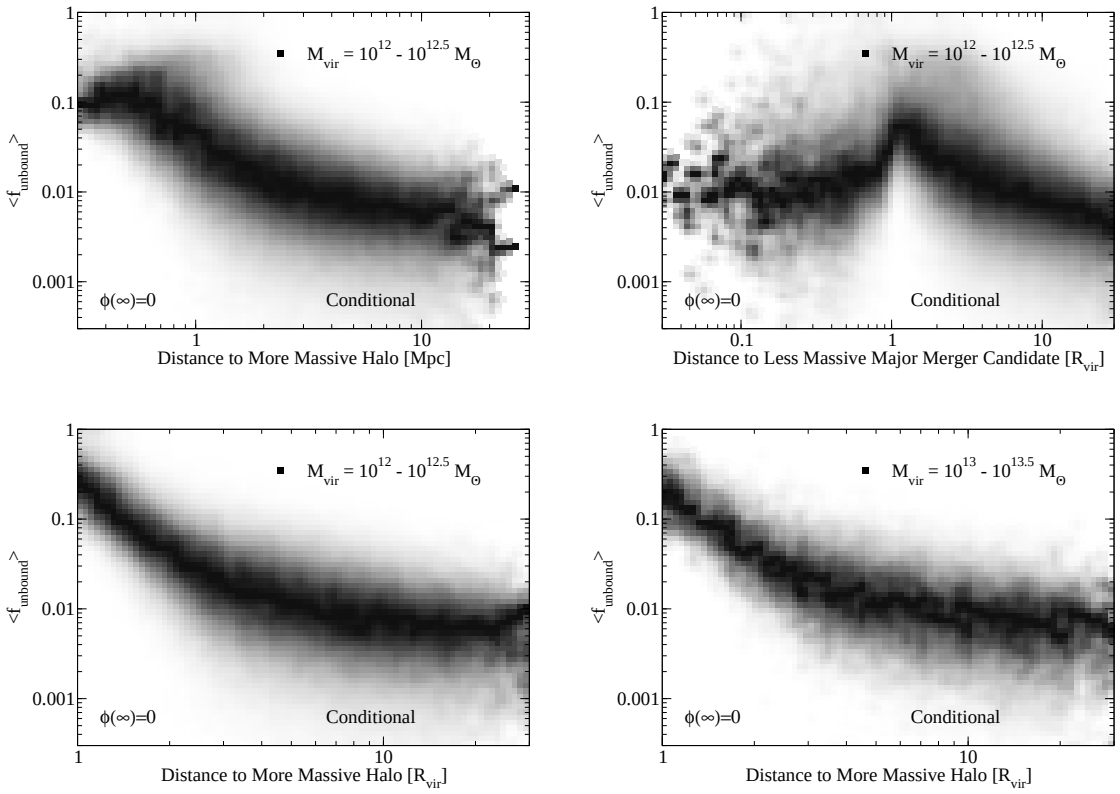

Figure 4. Halos in denser environments have larger unbound fractions. **Top-left panel**: The conditional probability distribution of the unbound fraction in $10^{12} - 10^{12.5} M_\odot$ halos as a function of the distance to the nearest larger halo. **Bottom-left panel**: Same as top-left panel, except now in units of the larger halo's virial radius. This shows that the unbound fraction for smaller halos climbs steeply within 3-4$R_{\rm vir}$ of a larger halo due to the larger background velocity dispersion. **Bottom-right** panel: same as bottom-left panel (the conditional probability distribution of the unbound fraction), except for group-scale ($10^{13} - 10^{13.5} M_\odot$ halos. **Top-right panel**: Unbound fraction in $10^{12} - 10^{12.5} M_\odot$ host halos as a function of the distance to the nearest major merger or major merger candidate, in units of the larger halo's virial radius. For ongoing major mergers, this distance will be less than one virial radius; for impending major mergers this distance will be more than one virial radius. Once the smaller halo crosses the virial radius of the larger halo, the unbound fraction drops swiftly. This is because the mass of the smaller halo is added to that of the larger halo once it crosses the virial radius, so that more and more particles are bound to the combined potential of the two halos.

the background velocity dispersion are responsible for the majority of the variation in the unbound fraction. Interpreted in the context of dark matter detection experiments, this suggests that the high-energy tail of the dark matter velocity distribution function may be substantially different for halos which are about to merge into a larger object as compared to field halos (i.e., halos which have no nearby neighbors of comparable size). For the Milky Way specifically, the nearest larger halo would be associated with M31, which is approximately three virial radii away [58]. The average unbound fraction for such halos is 2.8%, practically identical to the 2.9% average for all halos in the same mass bin. The Milky Way is thus not

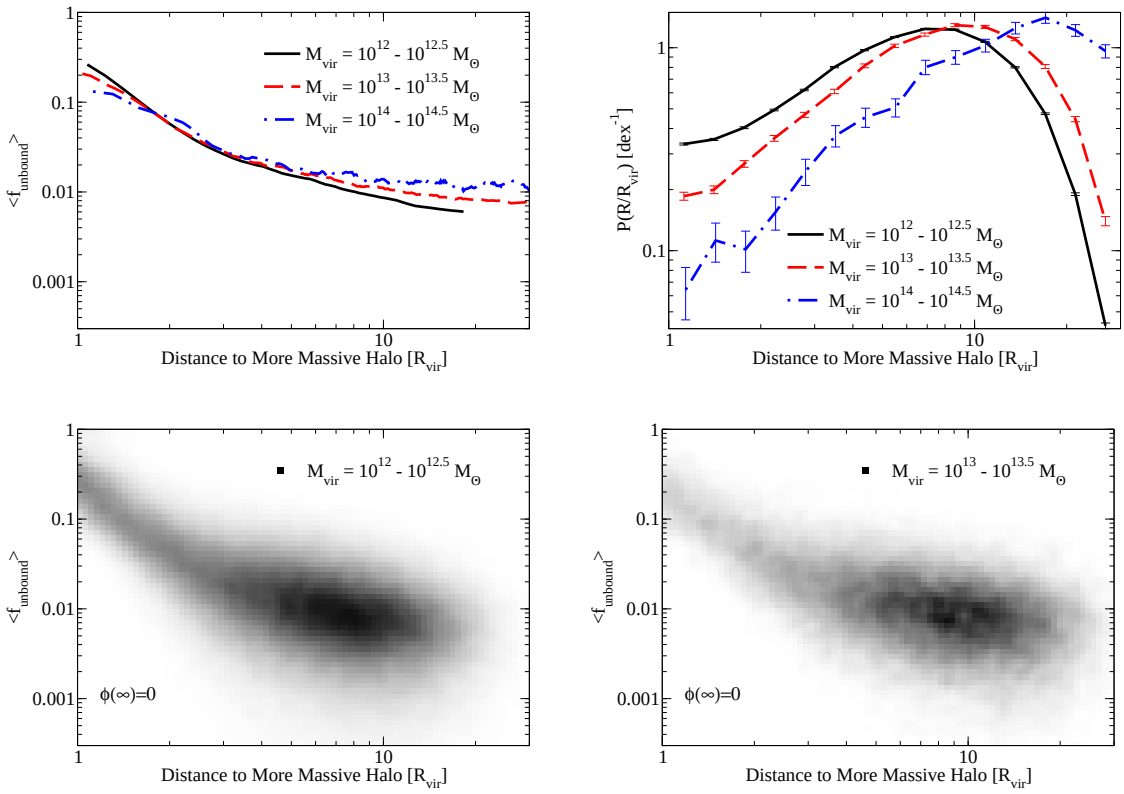

Figure 5. The **top left** panel shows the average unbound fraction for halos as a function of the distance to the nearest larger halo, scaled by the larger halo's virial radius (analogous to the bottom panels of figure 4). The environmental trend substantially dominates over the mass trend. The **top right** panel shows the probability distribution for the distance to the nearest larger halo in bins of halo mass. Unsurprisingly, it is more common for larger halos to be the largest object in their vicinity, and therefore not subject to tidal effects which would increase the number of unbound particles. **Bottom panels**: the absolute, as opposed to conditional, probability distribution for the unbound fraction as a function of distance to the nearest larger halo (compare to figure 4, bottom panels).

expected to have a particularly unusual velocity distribution based on its environment.

In light of the clear environmental dependence of the unbound fraction, it may be surprising that halos in major mergers showed comparatively small increases in the unbound fraction in figure 2. However, as mentioned previously, particles in one halo which cross the virial radius of another will contribute to the virial mass of the second halo. Thus, although a major merger is contributing unbound particles, it is also contributing a significant amount to the gravitational potential as well. To explore the balance between these two effects, the top-right panel of figure 4 shows the unbound fraction in Milky Way-sized halos as a function of the distance to the nearest smaller halo with $v_{\rm max,smaller} > 0.6 v_{\rm max,larger}$. In this panel, there is a very clear increase in the unbound fraction as the smaller halo approaches the larger one; however, as soon as it begins to contribute a significant amount of mass to the larger halo, the unbound fraction rapidly drops back down to nearly the field halo value. At the same time, once the smaller halo crosses the virial radius of the larger halo, the majority

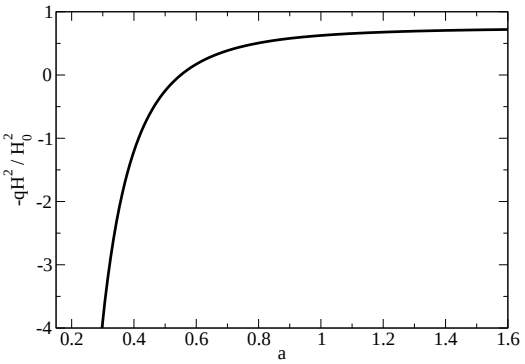

Figure 6. The evolution of $-qH^2$ with scale factor, relative to H_0^2. Negative values imply that the Hubble flow decelerates escaping particles; escape to infinity is impossible while this is the case (see Eq. (3.2)). Positive values of $-qH^2$ imply that the Hubble flow accelerates escaping particles. The transition between these states occurs at $a = 0.55$ for our chosen cosmology. In the far future, $-qH^2$ asymptotes to $\Omega_\Lambda H_0^2$.

of the unbound particles which are going to enter the larger halo have already done so. Since they are unbound, they will rapidly leave the halo, depleting the high-energy tail of the velocity function during the time it takes the smaller halo to sink to the center of the larger one.

It should be noted that the dependence of the average unbound fraction on environment for larger halos is very similar to that for Milky Way-size halos (figure 5, top left panel), although the field value rises slightly with halo mass. To fully explain the wider scatter seen in the probability distribution in figure 1, we note that smaller halos are much more likely than larger halos to have a nearby larger neighbor (figure 5, top right panel). The environmental impact of a larger neighbor on the unbound fraction is very strong when it is within 1-3 virial radii, which leads to a greater scatter overall in Milky Way-sized halos. From the bottom panels of figure 4, group-scale halos are more likely than Milky Way-sized halos to be the largest halo in their nearby environment, and so are less likely to have high unbound fractions, and the same trend holds for cluster-scale halos as well.

3.2 Energy Thresholds for Particle Ejection

3.2.1 Analytic Modeling

As mentioned in §2.3, setting $\phi(\infty) = 0$ in Eq. (2.1) ignores the effects of gravity in an expanding universe. Of course, particles in a cosmological halo can easily transfer energy and angular momentum through interactions with substructure, so it is perhaps besides the point to seek a better analytical solution for particle boundedness. Nonetheless, doing so provides a way to better understand how many and which particles could be expected to leave the halo and never return in an N-body simulation.

If one considers a point mass in an expanding cosmology, the effective acceleration a_t experienced by a test particle moving radially with respect to the point mass will be [59]:

$$a_t = \left(-\frac{GM}{r^2} - qH^2 r \right) \hat{r} \tag{3.2}$$

where M is the value of the point mass, H is the Hubble expansion rate ($\dot{a}a^{-1}$), and q is the deceleration parameter ($-\dot{H}H^{-2} - 1 = -\ddot{a}a^{-1}H^{-2}$). Both q and H evolve with time; the

evolution of the product $-qH^2$ for our chosen cosmology is shown in figure 6.

At early times ($a < 0.55$), $-qH^2$ is negative, and it is impossible for the test particle to escape to infinity. This is because the deceleration scales linearly with distance: the farther the test particle gets, the stronger the deceleration it experiences. However, at later times ($a > 0.55$), $-qH^2$ becomes positive, and it becomes easier and easier to escape. At very late times, the expansion of the universe becomes exponential (constant H), implying $q \to -1$. Therefore, the product $-qH^2$ approaches a final value of $\Omega_\Lambda H_0^2$ (see also [60]), as may be seen from the evolution of H in a flat universe:

$$H^2(a) = H_0^2(\Omega_M a^{-3} + \Omega_\Lambda). \tag{3.3}$$

However, the complexity of the time evolution of qH^2 means that there is little pedagogical value in solving the equation of motion (Eq. (3.2)) exactly. Instead, it is useful to consider the late-time limit, i.e., that qH^2 is approximately constant. As may be seen in figure 6, this is a good approximation even at the present day; $qH^2 = -0.63H_0^2$ at $z = 0$ and changes only by $\sim 10\%$ in the next 3 Gyr.

Supposing that a test particle has a boundedness b, the initial velocity will be

$$v_0 = \sqrt{\frac{(1-b)2GM}{r_0}} \tag{3.4}$$

and the velocity as a function of radius will be

$$v(r) = \sqrt{2GM\left(\frac{1}{r} - \frac{b}{r_0}\right) - qH^2(r^2 - r_0^2)} \tag{3.5}$$

If there is a solution to the equation $v(r > 0) = 0$, then the particle will be bound. While it is simple to solve the resulting cubic equation in r mathematically, a more instructive solution may be obtained intuitively. Within the equivalence radius r_e, defined as

$$r_e = \sqrt[3]{\frac{GM}{-qH^2}}, \tag{3.6}$$

the gravitational force will dominate and the particle will slow down; however, for $r > r_e$, the Hubble acceleration will dominate and the particle will speed up. Hence, if $v(r_e)$ is positive, the particle will escape to infinity; if $v(r_e)$ is zero or imaginary, then the particle will never pass beyond r_e and will therefore be bound. The resulting boundedness condition is therefore

$$2GM\sqrt[3]{\frac{-qH^2}{GM}} - \frac{2GMb}{r_0} - qH^2\left[\left(\frac{GM}{-qH^2}\right)^{\frac{2}{3}} - r_0^2\right] \leq 0 \tag{3.7}$$

This may be readily simplified to obtain

$$b \geq \frac{r_0}{2GM}\left(-3\sqrt[3]{q}(GMH)^{\frac{2}{3}} + qH^2 r_0^2\right) \tag{3.8}$$

Thus, for any particular choice of initial parameters, it can be quickly verified if the particle escapes or not.

While Eq. (3.8) only holds for point masses, it is easy to generalize this result. Specifically, we may note that the following is a conserved quantity for a test particle:

$$E_h = KE + PE + \frac{1}{2}qH^2r^2 = bPE + \frac{1}{2}qH^2r^2 \tag{3.9}$$

where KE is the physical kinetic energy per unit mass and PE refers to the Newtonian potential. Approximating a halo as a spherically-symmetric matter distribution truncated at the virial radius (especially valid at late times [61]), we note that Eq. (3.8) can be translated using Eq. (3.9) to any radius within the halo as:

$$E_h \leq -\frac{3\sqrt[3]{q}}{2}(HGM_{\rm vir})^{\frac{2}{3}} \tag{3.10}$$

where we have used $-GM_{\rm vir}R_{\rm vir}^{-1}$ as the Newtonian potential at the halo boundary.[3]

Unlike in a Newtonian potential, the escape speed threshold will depend on the particle's trajectory. For non-radial orbits, the particle will have some angular momentum; thus, for example, there will be a minimum velocity required at the equivalence radius to conserve angular momentum. Specifically, the quantity rv_t will be conserved, where v_t is the tangential component of the particle's velocity. However, obtaining the boundedness condition in this case requires solving a quartic equation, so the solution is presented in appendix A in Eq. (A.6).

Eqs. (3.10) and (A.6) are straightforward and simple tests for boundedness. If an alternate mass definition is desired, one needs only replace $M_{\rm vir}$ with the appropriate halo mass. If the potential energy is not available for a particle, it may be estimated using Eq. (B.3) in appendix B, which gives the Newtonian potential for a particle relative to a [56] halo profile.

It is worthwhile to note that Eq. (3.10) and (A.6) predict significantly different requirements on boundedness than for the Newtonian case. For example, a test particle at the virial radius of a halo at $z = 0$ could escape on a radial trajectory even if its kinetic energy was 34% less in magnitude than its Newtonian potential energy ($b = 0.34$)! A particle with a purely tangential initial velocity would require slightly over 6% more kinetic energy to escape, meaning that any particle at the virial radius with $b < 0.29$ could escape the halo. If the particle were instead at the halo center, the boundedness threshold would depend on concentration. Eq. (B.3) would suggest that for a massive halo with concentration c between $3 - 5$, the potential energy at the center would be $3 - 4$ times that at the halo radius; this would mean that the boundedness threshold would tighten to $b < 0.084$ to $b < 0.11$ to escape from the halo center at $z = 0$.

Note that, in the late-time limit, the halo mass does not change with time, as all the nearby matter has already been accreted [62]. As discussed in §3.2.2, the correction even at $z = 0$ due to the accretion rate of halos is significant, meaning that the true energy threshold for escape for particles in a given halo will depend on the individual halo's future mass accretion.

3.2.2 Numerical Simulations

To investigate the accuracy of the boundedness thresholds derived in the previous section, we now turn to numerical simulations of a more realistic model of the halo environment.

[3] Note that this assumes that the equivalence radius is beyond the virial radius, which is readily verified.

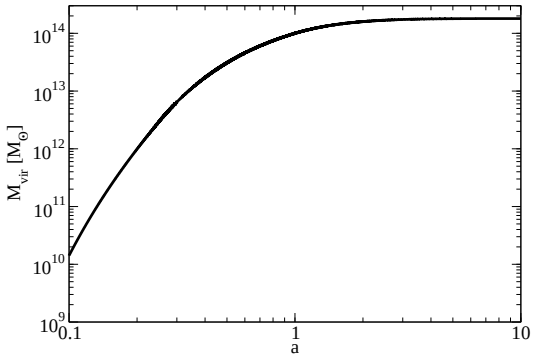

Figure 7. The mass accretion history and future for a $10^{14} M_\odot$ halo at $z = 0$ as given by Eqns. (3.12)-(3.14). Beyond a scale factor of $a = 3$, further accretion is practically negligible.

Specifically, we relax the assumption that the acceleration term $-qH^2$ remains fixed, and instead allow it to evolve using Eq. (3.3) and the standard equation for the scale factor $a(t)$ in a flat universe:

$$a(t) = \sqrt[3]{\frac{\Omega_m}{\Omega_\Lambda} \sinh^2 \left(\frac{3}{2} H_0 t \sqrt{\Omega_\Lambda} \right)} \tag{3.11}$$

We adopt $\Omega_m = 0.25$, $\Omega_\Lambda = 0.75$, and $H_0 = 70$ km s^{-1} Mpc^{-1} for consistency with the cosmological simulation we have used.

As mentioned at the end of §3.2.1, halos are always in the process of accreting matter, so the gravitating mass affecting an escaping particle will be changing as well. For these numerical simulations, we model halos as having spherical [56] profiles with concentrations given by [63] and mass accretion histories accounted for by a slight modification to the standard formula from [64]:

$$M_{\rm vir}(a) = M_0 \exp(z f(M_0, a)) \tag{3.12}$$

We allow the extra dependence on redshift on account of the fact that the far future mass accretion rates are somewhat less than those predicted by the mass accretion histories in [64]. Specifically, based on the mass accretion histories to $a = 100$ in [62] and the mass accretion histories for $a \leq 1$ from the merger trees in [52], we adopt the following functional form for $f(M_0, a)$:

$$\begin{aligned} f(M_0, a) = g(a) \Bigg[& -0.122 \log_{10} \left(\frac{M_0}{10^{6.47} M_\odot} \right) \\ & -0.328 \exp \left(\log_{10} \frac{M_0}{10^{14.24} M_\odot} \right) \Bigg] \end{aligned} \tag{3.13}$$

$$g(a) = \begin{cases} 1 \text{ if } a \leq 1 \\ 0.5 + 0.5 \left(\frac{2}{1+a} \right)^{1.3} \text{ if } a > 1 \end{cases} \tag{3.14}$$

An example of the mass accretion history (and future) for a $10^{14} M_\odot$ halo at $z = 0$ is shown in figure 7.

With these assumptions, we can more realistically evaluate the trajectory of a particle released in a cosmological environment. An important caveat remains, however, which is the

assumed definition of "unbound." As mentioned in the previous section, *no particle with finite energy can ever escape to infinity* as long as the deceleration parameter q is positive. However, high-energy particles can still escape by waiting until such a time as the deceleration parameter becomes negative (for $a > 0.55$), whereupon it becomes possible to leave the halo. We therefore define "unbound" as "can escape to infinity at some time in the future." This is well-defined but not trivially so: all halos will eventually stop accreting, and qH^2 will eventually asymptote to $-\Omega_\Lambda H_0^2$. As such, there will be a well-defined equivalence radius (Eq. (3.6)) which will asymptote to a constant multiple of the virial radius as $t \to \infty$; particles which remain within that radius will stay bound, whereas particles which remain outside that radius will escape.

Another important consideration is the gravitational potential which is used to evaluate the motion of particles. Halos are widely thought of as "gravitationally bound objects" [49]. Yet, halos do not exist in isolation, and there is a considerable extent of nearby matter which contributes to the gravitational potential well (see, e.g., [62]). There are thus two reasonable interpretations of "boundedness": one, that a particle cannot escape from the gravitational potential of matter assigned to the halo (e.g., matter within the virial radius); or two, that a particle cannot escape from the associated cosmological environment of the halo. We consider both definitions, the first corresponding to simulations where we truncate the halo density profile at the virial radius ("Virial Potential"), and the second corresponding to a truncation of the halo density profile where it matches the critical density of the Universe ("Full Potential").

We show results from the numerical simulations for the mass-dependence of the boundedness threshold at $z = 0$ in the top panel of figure 8. It is apparent that the mass accretion rates of halos represent a non-trivial correction to the result of Eq. (3.8). For smaller halos, which accrete less rapidly, the boundedness threshold approaches the value $b = 0.34$ derived for a constant halo mass and value for qH^2. For larger halos, which accrete more rapidly, more kinetic energy is necessary to counteract the future increase in the depth of the gravitational potential well. Also, as may be expected, more kinetic energy is necessary to escape from the full cosmological environment of the halo as opposed to the halo itself.

As shown in the middle panel of figure 8, the boundedness threshold varies substantially with radius. At $r = 0$, the change in the potential energy barrier due to the expansion of the Universe is relatively small, so the boundedness threshold approaches the Newtonian limit of $b = 0$. At $z = 0$, the Universe is accelerating, so particles at larger radii require less kinetic energy to escape. However, also at larger radii, the gravitational potential calculated from matter within the virial radius (which is used in the definition of b) more severely underestimates the full potential of all the matter in the halo's environment. This contributes to a feature in the boundedness threshold out to $R \sim 1.5R_{\rm vir}$ (at $z = 0$); if b were calculated using the full potential instead of the virial potential, then the boundedness threshold for the full potential would also rise monotonically with radius. At $z = 1$, the Universe is decelerating; moreover, particles at larger radii feel the effects of deceleration more strongly. However, particles at larger radii will also eventually feel more effects from acceleration after $a = 0.6$; hence, the variation of the boundedness threshold with radius is not monotonic for either the virial potential or full potential case.

Finally, the bottom panels of figure 8 show how the boundedness threshold varies with scale factor. At early times ($a < 0.6$), the deceleration of the Universe as well as the rapid rate of accretion means that it is very difficult to escape from halos. At very early times, this is especially severe; at $z = 4$, for example, the traditional definition of an unbound particle

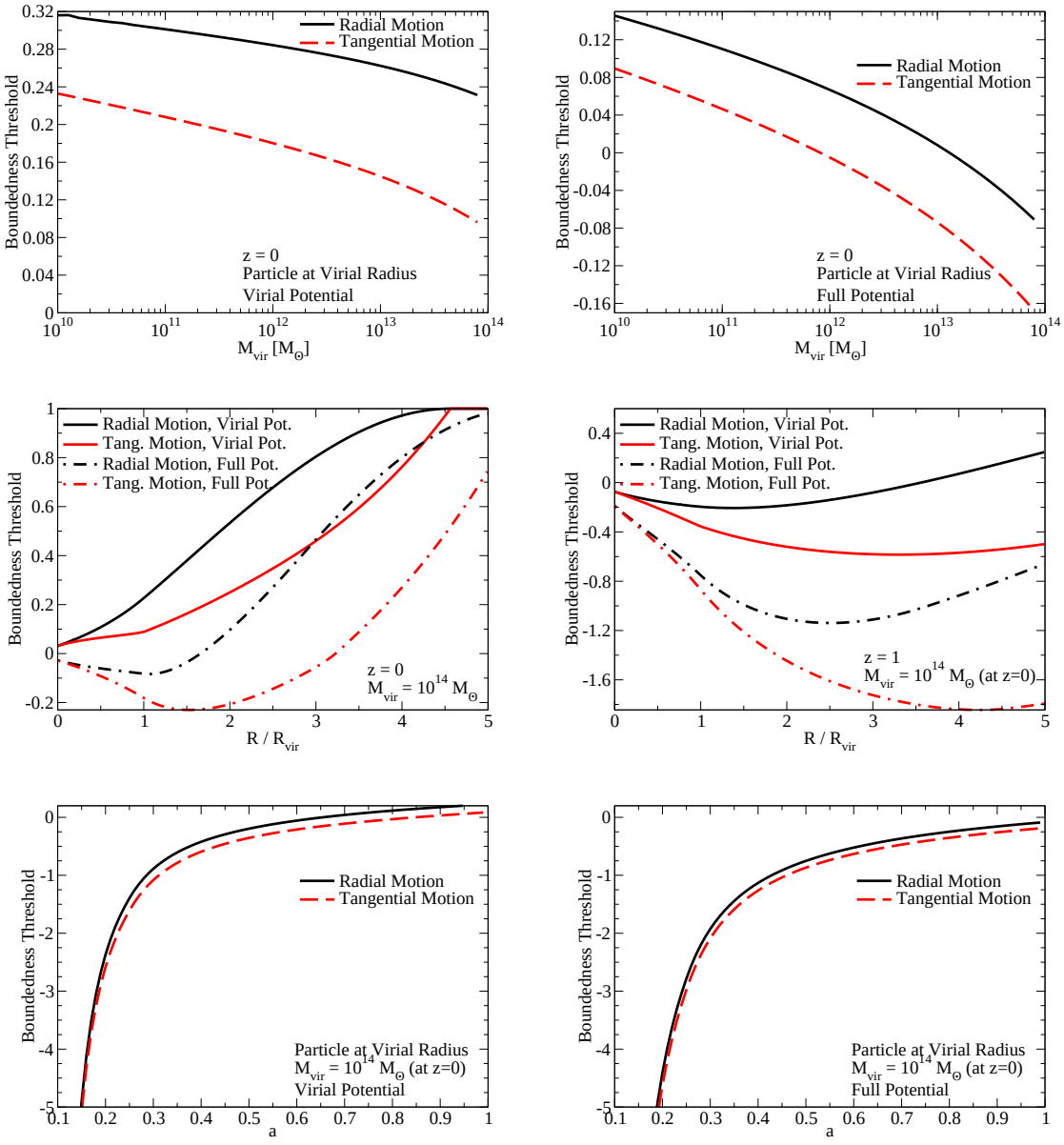

Figure 8. Boundedness thresholds (b, Eq. (2.3)) for particles relative to the potential of the host halo ("Virial Potential") and to the potential of the full cosmological environment ("Full Potential"). A boundedness of $b = 0$ corresponds to the traditional definition of boundedness, where the current kinetic energy equals the current Newtonian potential energy from the associated halo (i.e., considering the potential contribution only from particles within the halo's virial radius). The **top panels** show that the boundedness thresholds vary with mass, in contrast to the result suggested by Eq. (3.8), because halo accretion rates vary significantly with mass. The **middle panels** show how boundedness thresholds vary with radius; at $r = 0$, the traditional definition is very close to being accurate, because the effective potential is dominated by gravitation from the halo itself. However, at larger radii, the effective potential is increasingly dominated by the expansion of the Universe, to the point that particles with very little kinetic energy in comparison to their potential energy ($b \to 1$) can still escape. Finally, the **bottom panels** show how the threshold varies with scale factor; while the Universe was decelerating ($a < 0.6$), it was much more difficult for particles to escape to infinity.

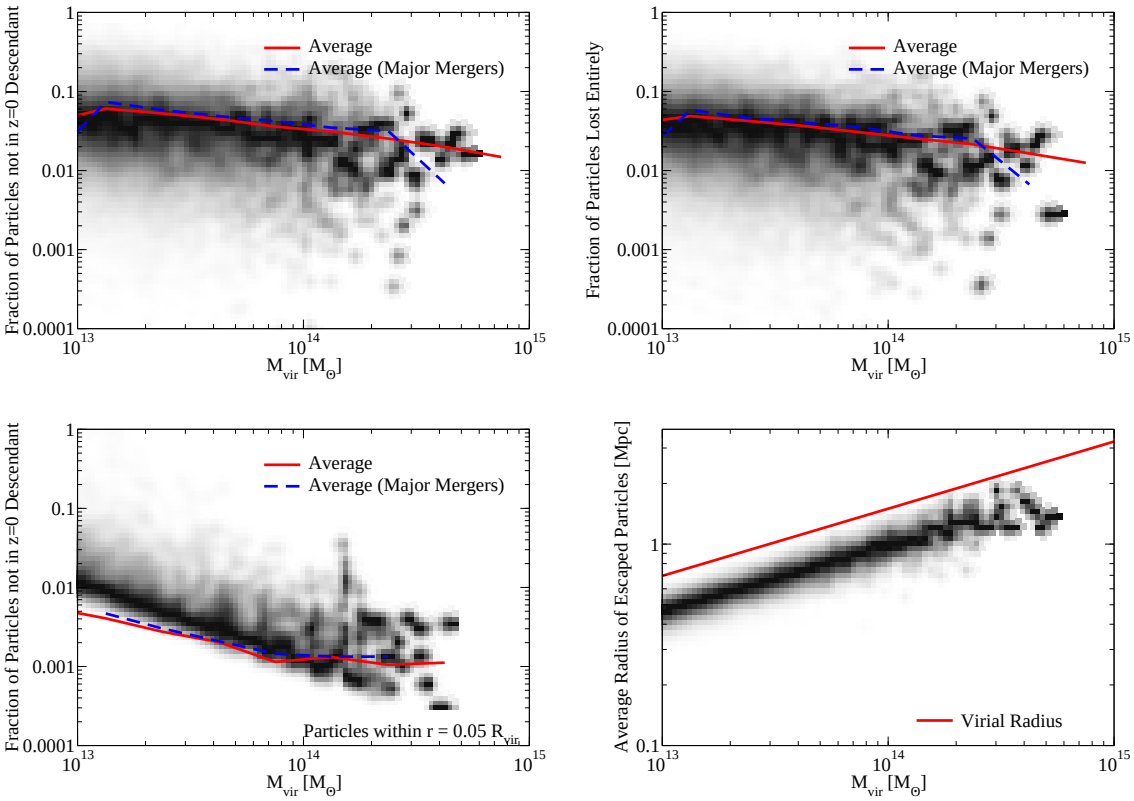

Figure 9. **Top left panel**: Approximately 2-10% of particles in halos above $10^{13} M_{\odot}$ at $z \sim 1$ do not appear in the $z = 0$ descendant. This panel shows the conditional probability density of the escape fraction as a function of halo mass at $z = 1$. **Top right panel**: While a significant fraction of particles in $z = 1$ halos do not appear in the $z = 0$ descendant, the fraction of particles which do not show up in *any* $z = 0$ halo (as opposed to the main descendant) is only slightly less. This plot shows the conditional probability density of the loss fraction as a function of halo mass at $z = 1$. **Bottom left panel**: for particles within 150 kpc (physical) of the halo center, the escape fraction is substantially less, especially for more massive halos. This agrees with the previous section's analysis that even marginally unbound particles are rare in the center of massive halos (see figure 2). **Bottom right panel**: for most halos, the average radius (at $z = 1$) of escaping particles between $z = 1$ and $z = 0$ is tightly clustered at around 70% of the virial radius. This panel shows the conditional probability distribution for individual halos at $z = 1$ for the average radius of particles lost between $z = 1$ and $z = 0$.

would underestimate the required kinetic energy for escape by a factor of $4 - 6$. This would imply that it is not advisable to remove "unbound" particles according to the traditional definition at high redshift; however, as shown in figures2 and 3, the error caused by doing so is small due to the rapidly dropping fraction of unbound particles.

3.3 Full Cosmological Simulations

We now turn to an analysis of which particles actually end up escaping in a full cosmological simulation. Since it is impossible to test whether a particle escapes to infinity without running the simulation to a very late time, we instead consider which particles can escape the virial

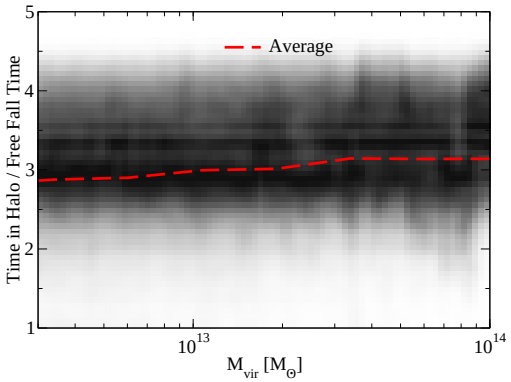

Figure 10. For particles which escape halos between $z = 1$ and $z = 0$, this plot shows the conditional probability density of the time that they spend in/around halos before escaping (see text), relative to the free fall time of the last halo they were in. On average, particles which escaped between $z = 1$ and $z = 0$ spent three free fall times in/around halos before they left.

radius of their host halos. To do so, we track particles in Consuelo between $z \sim 1$ and $z = 0$ to see which of them actually remain in the halo with which they were associated at $z = 1$. Specifically, for every progenitor halo at $z = 1$, we can find the descendant halo at $z = 0$ which receives the largest fraction of the progenitor's particles. The progenitor particles which do not end up in the descendant may then be assumed to have escaped sometime between $z = 1$ and $z = 0$.

Figure 9 shows the results of this analysis; most halos lose about 2-10% of their particles between $z \sim 1$ and $z = 0$. This is intermediate between the fraction of particles which can escape to infinity (2-3%) and the fraction which can pass beyond the halo radius (30%) calculated in §3.1. Intuitively, this may be explained by the fact that halos continually grow between $z \sim 1$ and $z = 0$, so that some of the particles which would be considered as having left the $z = 1$ halo radius would be counted as being within the $z = 0$ halo radius. Another possibility is that particles could be scooped up by passing halos and end up in a different descendant at $z = 0$; however the top-right panel of figure 9 suggests that this happens for only 15-20% of the escaped particles, and that the majority still end up not in any halo at $z = 0$. As shown in figure 9, halos which undergo major mergers between $z = 0$ and $z \sim 1$ (defined as cases where two progenitor halos at $z = 1$ which have a $v_{\rm max}$ ratio of at least 1:0.6 share the same $z = 0$ descendant) do not have substantially higher loss fractions.

Considering particles only within the inner 5% of the virial radius (figure 9, bottom left panel), the escape fraction is substantially smaller and largely similar to the unbound particle fraction within the same radius. In addition, the average radius of particles which have escaped between $z \sim 1$ and $z = 0$ is roughly 70% of the virial radius; this is significantly larger than the average particle radius, which is roughly 40-50% of the virial radius for halos in figure 9.

3.4 Origins of Ejected Particles

We can gain additional information about escaping particles by considering their origins as well as the amount of time they spend in and around halos before being ejected. For this analysis, we follow approximately 40 million particles in a subvolume of Consuelo (1/64 of the total volume) at every timestep from $a = 0.075$ to $a = 1$ and tag particles as either: (a) not associated with a halo, (b) smoothly accreted onto its current halo, or (c) initially

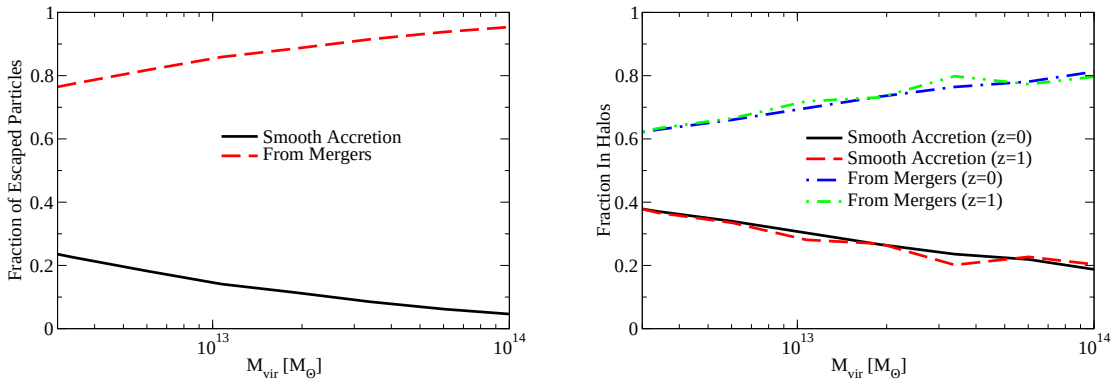

Figure 11. The origins of most escaped particles are from mergers. **Left panel**: The fraction of escaped particles (between $z = 1$ and $z = 0$) which arrived in mergers as compared to the fraction which arrived via smooth accretion. **Right panel**: The fraction of particles within $z = 0$ and $z = 1$ halos which entered the halo via smooth accretion and via mergers.

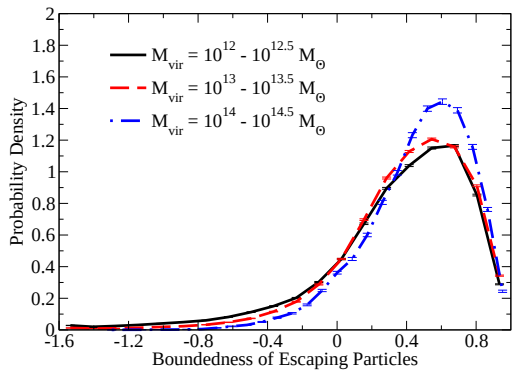

Figure 12. The distribution of boundedness levels for particles which leave halos between $z = 1$ and $z = 0$, for the assumption that $\phi(\infty) = 0$. Most particles are bound enough that they will never escape the halo; their orbit simply takes them outside of the virial radius. However, a small fraction of escaping particles have enough energy to never return, even in the far future.

belonging to a different halo and merging into its current halo. We also tag major mergers and cases where the particle leaves the virial radius of its current halo and either returns at a later time or enters into a new halo.

Relevant to the previous section, we limit our analysis to particles which enter halos before $z = 1$ and leave at some point before (but do not return by) $z = 0$. For each particle, we calculate the time it spent in/around halos (i.e., the last time it appeared in a halo minus the first time it appeared in a halo) relative to the free fall time of the last halo it was in ($\sqrt{2R^3(GM)^{-1}}$). Figure 10 shows the conditional probability distribution of this time for escaped particles in this analysis as a function of the mass of the last halo they were in. Regardless of host halo mass, escaped particles spent on average three free fall times in/around halos before escaping, corresponding to slightly less than a full orbital period. We have verified that this does not depend on whether the last halo the particle was in was undergoing a major merger.

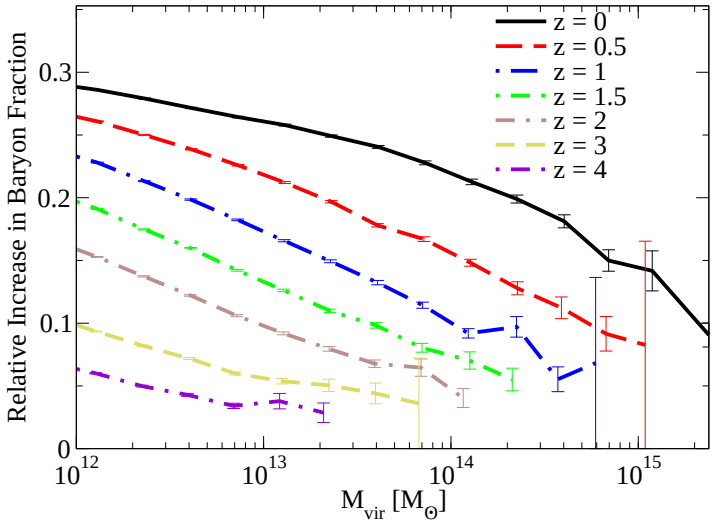

Figure 13. High-energy incoming baryons will collide with existing gas and remain inside halos, whereas high-energy incoming dark matter particles will escape. This will enhance the baryon fraction over the cosmic average; this figure shows the relative increase in the baryon fraction as a function of halo mass and redshift due to this effect. For small halos, baryonic feedback effects (such as supernovae and stellar winds) overwhelm the importance of this effect and decrease the baryon fraction below the cosmic average. However, this effect may be more important on the outskirts of massive halos, where feedback effects will be less important. Errors shown are jackknife uncertainties in the average across halos at a given mass and redshift.

As shown in the left panel of figure 11, the vast majority of escaping particles came in via mergers, as opposed to smooth accretion. The exact fraction is necessarily resolution-dependent; we have verified, however, the expected behavior that lowering the resolution of the simulation results in a larger smooth accretion fraction. By comparing to the origins of particles within the virial radius for halos at $z = 0$ and $z = 1$ (figure 11, right panel), particles which came in via mergers are much more likely to escape the halo as compared to particles which came in via smooth accretion.

Taken together with the results in previous sections, these results suggest that mergers are indeed responsible for ejecting most particles from halos. Although the ejection efficiency must decrease for extremely minor mergers, major mergers do not appear to be any more effective in ejecting particles than moderate and minor mergers. Finally, we note that the majority of escaped particles will eventually return. We show the boundedness distribution for escaped particles in figure 12; by comparison the escape thresholds in figure 8, it is clear that most of the escaped particles do not have sufficient energy to leave the halo's potential well completely.

3.5 The Effect of Unbound Particles on the Baryon Fraction

As mentioned in the introduction, high-energy dark matter particles can freely pass through dark matter halos, whereas high-energy baryons will shock against the hot halo gas and remain inside the halo. This effect will be balanced by galaxy outflows and other baryonic feedback effects which will tend to drive baryons out of the halo. These latter effects are especially important for lower-mass halos ($M_h < 10^{14} M_\odot$), where the energy transfer in feedback effects can be comparable to the binding energy of the baryons. However, in high-

mass clusters ($M_h > 10^{14} M_\odot$), the binding energy is large enough that it is very difficult for baryons to escape the halo once they are accreted.

To estimate the effects due to the different collisionalities of baryons and dark matter, we evaluate a toy model on all particles in the Consuelo simulation. For dark matter particles which are not contained in a halo, we assign the associated baryons (i.e., the cosmic baryon fraction times the particle mass) to the last halos in which the particles appeared, if any. Then, for all halos, we evaluate the ratio of assigned baryon mass to halo mass to calculate the relative increase in the baryon fraction from the collisionality effect.

This model serves to put an upper limit on the baryon fraction increase from this effect; predictions for the relative increase in the baryon fraction as a function of halo mass and redshift are shown in figure 13. There is a strong trend towards larger increases in the baryon fraction for smaller halos, which may be partially due to environmental effects (§3.1.2). As shown in figure 5, smaller halos are less likely to be the largest halo in their nearby environment. A nearby, larger neighbor will increase the nearby particle velocity dispersion as well as the relative impact velocity of merging satellites—increasing the fraction of unbound particles. In addition, because of tidal forces from the larger neighbor, a dark matter particle which leaves the immediate vicinity of the halo is unlikely to return. The relative change in the baryon fraction also increases at later redshifts; this may be related to the smaller fraction of unbound particles at high redshifts (figures 2 and 3) as well as the increasing ease of escape at later times due to the acceleration of the universe (figure 8).

Overall, at $z = 0$, the relative increase in the baryon fraction is between 15-30%, in qualitative agreement with the 25% implied by the results of [57] for Friends-of-Friends halos.[4] For very massive halos, this would suggest an average baryon fraction of nearly 0.19 within the virial radius at $z = 0$, instead of the cosmic baryon fraction of 0.16 for our assumed cosmology. For smaller halos, we cannot make concrete predictions due to the importance of baryonic feedback effects.

4 Discussion and Implications

From the perspective of individual particles, the virial radius of a halo is not special; as we and others [57] have found, roughly a quarter of the mass of dark matter halos at $z = 0$ has entered and left through this radius. Instead, the most important radius for the individual trajectory of particles is the equivalence radius (Eq. (3.6)), beyond which the Hubble flow will accelerate the particle away from the gravitational pull of the halo. At early times ($a < 0.55$), the deceleration of the universe makes it impossible for particles to completely escape from halos. However, at late times, the acceleration of the universe brings the equivalence radius from infinity down to roughly four times the virial radius. This leads to the creation of "islands" at late times ($a \gg 1$), whereby particles (and, indeed, other halos) which are not within the equivalence radius are expanded away at rates that gravity cannot overcome (see also [60, 62]).

We have shown that the fraction of unbound particles (regardless of definition) is a strong function of distance to the halo center as well as the host halo's environment (§3.1 and 3.1.2). Perhaps surprisingly, major mergers do not contribute substantially on average to the unbound fraction of particles. A major merger at the virial radius causes a substantial increase in the unbound fraction, but as the merger passes within the virial radius, its mass

[4] While [57] did not make the association to baryon fraction increases, their calculation of total halo masses is mathematically identical to that of our toy model.

also contributes to the gravitational potential, which raises the kinetic energy necessary for a particle to be considered unbound (§3.1.2). The strong environmental dependence that we find for the unbound fraction—which is linked to the high-energy tail velocity distribution function within halos—is relevant for interpreting dark matter detection experiments. However, we have verified that the nearby environment of the Milky Way (i.e., the presence of M31) barely changes its expected unbound fraction from the overall average for halos of the same mass.

In terms of precision calibrations of the dark matter halo mass function, we have noted that the cosmic baryon fraction will not correspond to the baryon fraction in halos even at very large radii (§3.5). This is because the ability of dark matter to freely pass beyond the virial radius of a halo is not shared by baryons. As the orbits of many dark matter particles take them beyond the virial radius (about a quarter of the mass that has ever been within a halo at $z = 0$), the baryons left behind will contribute to an excess beyond the cosmic baryon fraction in the halo.

This contribution is mass-dependent, but it is difficult to make concrete predictions for the baryon fraction for halos smaller than $10^{14} M_{\odot}$ due to the effects of stellar and quasar feedback being important for these halos. However, for high mass halos $M_h > 10^{14} M_{\odot}$, we find a redshift-dependent excess in the baryon fraction on the order of 5–15% (i.e., an observed baryon fraction of 0.17–0.19), as discussed in §3.5. This redshift dependence is important for observations of clusters, as a changing baryon fraction might otherwise be interpreted as an evolving dark energy parameter [65]. Encouragingly, similar trends for how the excess baryon fraction evolves with halo mass and redshift are observed in recent hydrodynamical simulations [34], although the overall normalization depends on the simulation code used.

Finally, regarding intergalactic supernovae, we find that it is difficult for central dark matter particles to acquire enough energy to leave their hosts (§3.3). Roughly 2-10% of particles within halos do so between $z = 1$ and $z = 0$, and the fraction drops by an order of magnitude for particles within the central 5% of the virial radius. Thus, depending on the host halo mass, the fraction of stars (i.e., supernovae progenitors) which receive enough of a kick in halo-halo mergers to leave the halo is on the order of a percent or less. Observations of hypervelocity supernovae above this fraction should correspond either to stars ejected via multi-body stellar interactions or to observational biases.

5 Conclusions

We have studied the properties of unbound particles as well as particles which have escaped from halos. Our main findings are as follows:

1. On average, at $z = 0$, 2–3% of particles in halos can escape to infinity, and 30% have enough energy to pass beyond the virial radius.

2. The fraction of unbound particles in halos is a steep function of distance from the halo center as well as environment (specifically, distance to the nearest larger halo). Comparatively, it is a weak function of halo mass and redshift.

3. Based on its halo mass, about $\sim 2.9\%$ of the Milky Way's dark matter is expected to be able to escape to infinity. The Milky Way itself appears to be typical in this sense; if priors about the distance between the Milky Way and Andromeda (M31) are included, this fraction changes negligibly. Priors on the distance to larger objects are

likely sufficient for determining the unbound fraction of particles contributing to the velocity distribution function of dark matter in halos, with relevance for interpretations of direct detection measurements.

4. In simulations, 2–10% of particles within dark matter halos at $z = 1$ escape and are not found within any other halo by $z = 0$. The vast majority of these escaped particles came in from merging satellites, as opposed to smooth accretion. Most of these escaped particles do not have enough energy to permanently leave and will return at some time in the future within the halo's virial radius.

5. The baryon fraction in massive (10^{14}–$10^{15} M_\odot$) halos may be boosted within the virial radius to 0.19 at $z = 0$ on account of unbound dark matter particles. This boost is redshift-dependent, leading to an expected baryon fraction of 0.175 at $z = 1$ for our assumed cosmology. The standard ΛCDM cosmological model thus generically predicts an evolving baryon fraction with redshift.

Acknowledgments

We are grateful to Michael Busha, who ran the Consuelo simulation used here, on the Orange cluster at SLAC. This was run as a part of the LasDamas collaboration simulations. We would also like to thank Dusan Keres for insightful discussions on baryon fractions in hydrodynamical simulations, and Tom Abel for useful discussions. This work received support from Stanford University and the U.S. Department of Energy under contract number DE-AC02-76SF00515.

A The Boundedness of a Test Particle For Arbitrary Trajectories

Knowing that the angular momentum rv_t will be conserved, we can write down the radial velocity v_r of a particle relative to a point mass as a function of its radius r:

$$v_r(r) = \sqrt{2GM\left(\frac{1}{r} - \frac{b}{r_0}\right) - qH^2(r^2 - r_0^2) - \left(\frac{r_0}{r} v_{t,0}\right)^2} \tag{A.1}$$

where $v_{t,0}$ is the original tangential velocity of the particle. For a halo, we can do the same outside of the virial radius, where we can write

$$v_r(r) = \sqrt{\frac{2GM}{r} - 2E_h - qH^2 r^2 - \left(\frac{r_0}{r} v_{t,0}\right)^2} \tag{A.2}$$

If the particle is unbound, then $v_r(r > 0) = 0$ can have at most one solution at $r \leq r_0$; a bound particle will have either a solution for $r > r_0$ or, in the case of a circular orbit, $r = r_0$ will be a solution and also a local maximum of v_r^2. One option for distinguishing these cases is to search for the zeros of the following quartic equation:

$$-qH^2 r^4 - 2E_h r^2 + 2GMr - r_0^2 v_{t,0}^2 = 0 \tag{A.3}$$

A somewhat simpler option is to search for the minimum of v_r^2 and check to see if it is negative; the locations of the extrema of v_r^2 are given by:

$$-2qH^2 r^4 - 2GMr + 2r_0^2 v_{t,0}^2 = 0 \tag{A.4}$$

Before solving this latter equation, recall that a particle on the threshold of boundedness will be one where v_r^2 just barely reaches zero; thus, the location of the minimum of v_r^2 and the location of the root will coincide at the turnaround radius. Hence, we can substitute Eq. (A.4) into Eq. (A.3) to reduce the equation to a quadratic:

$$E_h r^2 + \frac{3}{2} GMr - r_0^2 v_{t,0}^2 = 0 \tag{A.5}$$

This gives a simple boundedness formula for E_h:

$$E_h < \frac{-\frac{3}{2} GMr + r_0^2 v_{t,0}^2}{r^2} \tag{A.6}$$

We use Ferrari's method to approach the quartic in Eq. (A.4). The solution is:

$$r = \frac{1}{2}\left(\sqrt{y} + \sqrt{-y + \frac{2GM}{-qH^2\sqrt{y}}}\right) \tag{A.7}$$

$$y = 2\left(\sqrt[3]{R} + \frac{K}{\sqrt[3]{R}}\right) \tag{A.8}$$

$$R = J + \sqrt{J^2 - K^3} \tag{A.9}$$

$$J = \frac{G^2 M^2}{16 q^2 H^4} = \frac{r_e^6}{16} \tag{A.10}$$

$$K = \frac{r_0^2 v_{t,0}^2}{-3qH^2} \tag{A.11}$$

Of course, there are three more solutions to the quartic; the full solution set is

$$r = \frac{1}{2}\left(\pm_1\sqrt{y} \pm_2 \sqrt{-y \pm_1 \frac{2GM}{-qH^2\sqrt{y}}}\right) \tag{A.12}$$

where the $\pm_1$ correspond to identical signs, and the $\pm_2$ is independent. However, the solution in Eq. (A.7) is the only one which corresponds to $r = r_e$ (the equivalence radius) for radial motion ($v_{t,0} = 0$).

These equations have been verified as correct in gravitational simulations of a particle escaping a halo. Admittedly, they are quite inelegant, and in some cases, a simpler expression may be desired. A useful *approximation* is to require that angular momentum be conserved at the equivalence radius; this results in the following condition for $v_{t,0} > 0$:

$$E_h \lesssim -\frac{3\sqrt[3]{q}}{2}(HGM_{\rm vir})^{\frac{2}{3}} + \frac{1}{2} r_0^2 v_{t,0}^2 \left(\frac{-qH^2}{GM_{\rm vir}}\right)^{\frac{2}{3}} \tag{A.13}$$

For a particle with purely tangential velocity at the virial radius of a halo, this gives the correct bound for E_h to within about 1%.

B The Newtonian Potential of an NFW Halo

Given an NFW halo [56] with characteristic density ρ and scale radius r_s, the enclosed mass at a radius r is

$$M(r) = 4\pi\rho r_s^3 \left[\ln\left(\frac{r_s + r}{r_s}\right) - \frac{r}{r + r_s}\right] \tag{B.1}$$

Thus, the change in potential from radius r_1 to radius r_2 is

$$\Delta\phi = \int_{r_1}^{r_2} \frac{GM(r)}{r^2} dr = -\frac{4\pi G\rho r_s^3}{r} \ln\left(\frac{r_s + r}{r_s}\right)\Bigg|_{r_1}^{r_2} \tag{B.2}$$

If the halo is considered truncated at the virial radius, the potential outside will be that of a sphere with the virial mass. Thus, the combined Newtonian potential as a function of radius is:

$$\phi(r) = \begin{cases} -\frac{GM_{\rm vir}}{r} & r \geq R_{\rm vir} \\ -\frac{dGM_{\rm vir}}{r} \ln\left(\frac{r_s+r}{r_s}\right)\Big|_{R_{\rm vir}}^{r} - \frac{GM_{\rm vir}}{R_{\rm vir}} & r \leq R_{\rm vir} \end{cases} \tag{B.3}$$

where d is the following constant:

$$d = \left[\ln\left(\frac{r_s + R_{\rm vir}}{r_s}\right) - \frac{R_{\rm vir}}{R_{\rm vir} + r_s}\right]^{-1} \tag{B.4}$$

and noting the following limit applies for $r \to 0$:

$$\lim_{r\to 0}\left[\frac{1}{r}\ln\left(\frac{r_s + r}{r_s}\right)\right] = \frac{1}{r_s} \tag{B.5}$$

References

[1] P. S. Behroozi, R. H. Wechsler, and H.-Y. Wu, *The Rockstar Phase-Space Temporal Halo Finder and the Velocity Offsets of Cluster Cores*, *arXiv:1110.4372* (Oct., 2011) [arXiv:1110.4372].

[2] Y. Mao, L. E. Strigari, R. H. Wechsler, et al., *Halo-to-Halo Similarity and Scatter in the Velocity Distribution of Dark Matter*, *PRL submitted* (2012).

[3] M. Lisanti, L. E. Strigari, J. G. Wacker, and R. H. Wechsler, *Dark matter at the end of the Galaxy*, Phys. Rev. D **83** (Jan., 2011) 023519, [arXiv:1010.4300].

[4] N. Afshordi, R. Mohayaee, and E. Bertschinger, *Hierarchy in the phase space and dark matter astronomy*, Phys. Rev. D **81** (May, 2010) 101301, [arXiv:0911.0414].

[5] C.-P. Ma, P. Chang, and J. Zhang, *Is the Radial Profile of the Phase-Space Density of Dark Matter Halos a Power-Law?*, *arXiv:0907.3144* (July, 2009) [arXiv:0907.3144].

[6] I. M. Vass, S. Kazantzidis, M. Valluri, and A. V. Kravtsov, *Evolution of Dark Matter Phase-Space Density Distributions in Equal-Mass Halo Mergers*, ApJ **698** (June, 2009) 1813–1825, [arXiv:0812.3659].

[7] M. Zemp, J. Diemand, M. Kuhlen, P. Madau, B. Moore, D. Potter, J. Stadel, and L. Widrow, *The graininess of dark matter haloes*, MNRAS **394** (Apr., 2009) 641–659, [arXiv:0812.2033].

[8] M. Vogelsberger, A. Helmi, V. Springel, S. D. M. White, J. Wang, C. S. Frenk, A. Jenkins, A. Ludlow, and J. F. Navarro, *Phase-space structure in the local dark matter distribution and its signature in direct detection experiments*, MNRAS **395** (May, 2009) 797–811, [arXiv:0812.0362].

[9] M. Maciejewski, M. Vogelsberger, S. D. M. White, and V. Springel, *Bound and unbound substructures in Galaxy-scale dark matter haloes*, MNRAS **415** (Aug., 2011) 2475–2484, [arXiv:1010.2491].

[10] M. Vogelsberger and S. D. M. White, *Streams and caustics: the fine-grained structure of Λ cold dark matter haloes*, MNRAS **413** (May, 2011) 1419–1438, [arXiv:1002.3162].

[11] E. Aprile, K. Arisaka, F. Arneodo, A. Askin, L. Baudis, A. Behrens, K. Bokeloh, E. Brown, T. Bruch, G. Bruno, J. M. R. Cardoso, W.-T. Chen, B. Choi, D. Cline, E. Duchovni, S. Fattori, A. D. Ferella, F. Gao, K.-L. Giboni, E. Gross, A. Kish, C. W. Lam, J. Lamblin, R. F. Lang, C. Levy, K. E. Lim, Q. Lin, S. Lindemann, M. Lindner, J. A. M. Lopes, K. Lung, T. Marrodán Undagoitia, Y. Mei, A. J. Melgarejo Fernandez, K. Ni, U. Oberlack, S. E. A. Orrigo, E. Pantic, R. Persiani, G. Plante, A. C. C. Ribeiro, R. Santorelli, J. M. F. Dos Santos, G. Sartorelli, M. Schumann, M. Selvi, P. Shagin, H. Simgen, A. Teymourian, D. Thers, O. Vitells, H. Wang, M. Weber, and C. Weinheimer, *Dark Matter Results from 100 Live Days of XENON100 Data*, *Physical Review Letters* **107** (Sept., 2011) 131302, [arXiv:1104.2549].

[12] G. Angloher, M. Bauer, I. Bavykina, A. Bento, C. Bucci, C. Ciemniak, G. Deuter, F. von Feilitzsch, D. Hauff, P. Huff, C. Isaila, J. Jochum, M. Kiefer, M. Kimmerle, J.-C. Lanfranchi, F. Petricca, S. Pfister, W. Potzel, F. Pröbst, F. Reindl, S. Roth, K. Rottler, C. Sailer, K. Schäffner, J. Schmaler, S. Scholl, W. Seidel, M. v. Sivers, L. Stodolsky, C. Strandhagen, R. Strauß, A. Tanzke, I. Usherov, S. Wawoczny, M. Willers, and A. Zöller, *Results from 730 kg days of the CRESST-II Dark Matter search*, *European Physical Journal C* **72** (Apr., 2012) 1971, [arXiv:1109.0702].

[13] R. Bernabei, P. Belli, F. Cappella, R. Cerulli, C. J. Dai, A. D'Angelo, H. L. He, A. Incicchitti, H. H. Kuang, J. M. Ma, F. Montecchia, F. Nozzoli, D. Prosperi, X. D. Sheng, and Z. P. Ye, *First results from DAMA/LIBRA and the combined results with DAMA/NaI*, *European Physical Journal C* **56** (Aug., 2008) 333, [arXiv:0804.2741].

[14] C. E. Aalseth, P. S. Barbeau, J. Colaresi, J. I. Collar, J. Diaz Leon, J. E. Fast, N. Fields, T. W. Hossbach, M. E. Keillor, J. D. Kephart, A. Knecht, M. G. Marino, H. S. Miley, M. L. Miller, J. L. Orrell, D. C. Radford, J. F. Wilkerson, and K. M. Yocum, *Search for an Annual Modulation in a p-Type Point Contact Germanium Dark Matter Detector*, *Physical Review Letters* **107** (Sept., 2011) 141301, [arXiv:1106.0650].

[15] Z. Ahmed, D. S. Akerib, S. Arrenberg, C. N. Bailey, D. Balakishiyeva, L. Baudis, D. A. Bauer, P. L. Brink, T. Bruch, R. Bunker, B. Cabrera, D. O. Caldwell, J. Cooley, P. Cushman, M. Daal, F. DeJongh, M. R. Dragowsky, L. Duong, S. Fallows, E. Figueroa-Feliciano, J. Filippini, M. Fritts, S. R. Golwala, D. R. Grant, J. Hall, R. Hennings-Yeomans, S. A. Hertel, D. Holmgren, L. Hsu, M. E. Huber, O. Kamaev, M. Kiveni, M. Kos, S. W. Leman, R. Mahapatra, V. Mandic, K. A. McCarthy, N. Mirabolfathi, D. Moore, H. Nelson, R. W. Ogburn, A. Phipps, M. Pyle, X. Qiu, E. Ramberg, W. Rau, A. Reisetter, T. Saab, B. Sadoulet, J. Sander, R. W. Schnee, D. N. Seitz, B. Serfass, K. M. Sundqvist, M. Tarka, P. Wikus, S. Yellin, J. Yoo, B. A. Young, and J. Zhang, *Dark Matter Search Results from the CDMS II Experiment*, *Science* **327** (Mar., 2010) 1619–, [arXiv:0912.3592].

[16] D. Schlegel, M. White, and D. Eisenstein, *The Baryon Oscillation Spectroscopic Survey: Precision measurement of the absolute cosmic distance scale*, in *astro2010: The Astronomy and Astrophysics Decadal Survey*, vol. 2010 of *arXiv:0902.4680*, p. 314, 2009. arXiv:0902.4680.

[17] The Dark Energy Survey Collaboration, *The Dark Energy Survey*, *astro-ph/0510346* (Oct., 2005) [astro-ph/0510346].

[18] D. Schlegel, F. Abdalla, T. Abraham, C. Ahn, C. Allende Prieto, J. Annis, E. Aubourg, M. Azzaro, S. B. C. Baltay, C. Baugh, C. Bebek, S. Becerril, M. Blanton, A. Bolton, B. Bromley, R. Cahn, P. . Carton, J. L. Cervantes-Cota, Y. Chu, M. Cortes, K. Dawson, A. Dey, M. Dickinson, H. T. Diehl, P. Doel, A. Ealet, J. Edelstein, D. Eppelle, S. Escoffier, A. Evrard, L. Faccioli, C. Frenk, M. Geha, D. Gerdes, P. Gondolo, A. Gonzalez-Arroyo, B. Grossan, T. Heckman, H. Heetderks, S. Ho, K. Honscheid, D. Huterer, O. Ilbert, I. Ivans, P. Jelinsky, Y. Jing, D. Joyce, R. Kennedy, S. Kent, D. Kieda, A. Kim, C. Kim, J. . Kneib, X. Kong, A. Kosowsky, K. Krishnan, O. Lahav, M. Lampton, S. LeBohec, V. Le Brun, M. Levi, C. Li, M. Liang, H. Lim, W. Lin, E. Linder, W. Lorenzon, A. de la Macorra, C. Magneville, R. Malina, C. Marinoni, V. Martinez, S. Majewski, T. Matheson, R. McCloskey, P. McDonald, T. McKay, J. McMahon, B. Menard, J. Miralda-Escude, M. Modjaz, A. Montero-Dorta, I. Morales, N. Mostek, J. Newman, R. Nichol, P. Nugent, K. Olsen, N. Padmanabhan, N. Palanque-Delabrouille, I. Park, J. Peacock, W. Percival, S. Perlmutter, C. Peroux, P. Petitjean, F. Prada, E. Prieto, J. Prochaska, K. Reil, C. Rockosi, N. Roe, E. Rollinde, A. Roodman, N. Ross, G. Rudnick, V. Ruhlmann-Kleider, J. Sanchez, D. Sawyer, C. Schimd, M. Schubnell, R. Scoccimaro, U. Seljak, H. Seo, E. Sheldon, M. Sholl, R. Shulte-Ladbeck, A. Slosar, D. S. Smith, G. Smoot, W. Springer, A. Stril, A. S. Szalay, C. Tao, G. Tarle, E. Taylor, A. Tilquin, J. Tinker, F. Valdes, J. Wang, T. Wang, B. A. Weaver, D. Weinberg, M. White, M. Wood-Vasey, J. Yang, X. Y. C. Yeche, N. Zakamska, A. Zentner, C. Zhai, and P. Zhang, *The BigBOSS Experiment*, *arXiv:1106.1706* (June, 2011) [arXiv:1106.1706].

[19] N. Kaiser, H. Aussel, B. E. Burke, H. Boesgaard, K. Chambers, M. R. Chun, J. N. Heasley, K.-W. Hodapp, B. Hunt, R. Jedicke, D. Jewitt, R. Kudritzki, G. A. Luppino, M. Maberry, E. Magnier, D. G. Monet, P. M. Onaka, A. J. Pickles, P. H. H. Rhoads, T. Simon, A. Szalay, I. Szapudi, D. J. Tholen, J. L. Tonry, M. Waterson, and J. Wick, *Pan-STARRS: A Large Synoptic Survey Telescope Array*, in *Society of Photo-Optical Instrumentation Engineers (SPIE) Conference Series* (J. A. Tyson and S. Wolff, eds.), vol. 4836 of *Society of Photo-Optical Instrumentation Engineers (SPIE) Conference Series*, pp. 154–164, Dec., 2002.

[20] P. Predehl, R. Andritschke, H. Böhringer, W. Bornemann, H. Bräuninger, H. Brunner, M. Brusa, W. Burkert, V. Burwitz, N. Cappelluti, E. Churazov, K. Dennerl, J. Eder, J. Elbs, M. Freyberg, P. Friedrich, M. Fürmetz, R. Gaida, O. Hälker, G. Hartner, G. Hasinger, S. Hermann, H. Huber, E. Kendziorra, A. von Kienlin, W. Kink, I. Kreykenbohm, G. Lamer,

I. Lapchov, K. Lehmann, N. Meidinger, B. Mican, J. Mohr, M. Mühlegger, S. Müller, K. Nandra, M. Pavlinsky, E. Pfeffermann, T. Reiprich, J. Robrade, C. Rohé, A. Santangelo, G. Schächner, T. Schanz, C. Schmid, J. Schmitt, R. Schreib, F. Schrey, A. Schwope, M. Steinmetz, L. Strüder, R. Sunyaev, C. Tenzer, L. Tiedemann, M. Vongehr, and J. Wilms, *eROSITA on SRG*, in *Society of Photo-Optical Instrumentation Engineers (SPIE) Conference Series*, vol. 7732 of *Society of Photo-Optical Instrumentation Engineers (SPIE) Conference Series*, July, 2010. arXiv:1001.2502.

[21] G. L. Pilbratt, J. R. Riedinger, T. Passvogel, G. Crone, D. Doyle, U. Gageur, A. M. Heras, C. Jewell, L. Metcalfe, S. Ott, and M. Schmidt, *Herschel Space Observatory. An ESA facility for far-infrared and submillimetre astronomy*, A&A **518** (July, 2010) L1, [arXiv:1005.5331].

[22] The Planck Collaboration, *The Scientific Programme of Planck*, *astro-ph/0604069* (Apr., 2006) [astro-ph/0604069].

[23] J. P. Gardner, J. C. Mather, M. Clampin, R. Doyon, M. A. Greenhouse, H. B. Hammel, J. B. Hutchings, P. Jakobsen, S. J. Lilly, K. S. Long, J. I. Lunine, M. J. McCaughrean, M. Mountain, J. Nella, G. H. Rieke, M. J. Rieke, H.-W. Rix, E. P. Smith, G. Sonneborn, M. Stiavelli, H. S. Stockman, R. A. Windhorst, and G. S. Wright, *The James Webb Space Telescope*, Space Sci. Rev. **123** (Apr., 2006) 485–606, [astro-ph/0606175].

[24] LSST Science Collaborations, P. A. Abell, J. Allison, S. F. Anderson, J. R. Andrew, J. R. P. Angel, L. Armus, D. Arnett, S. J. Asztalos, T. S. Axelrod, and et al., *LSST Science Book, Version 2.0*, *arXiv:0912.0201* (Dec., 2009) [arXiv:0912.0201].

[25] H. Wu, A. R. Zentner, and R. H. Wechsler, *The Impact of Theoretical Uncertainties in the Halo Mass Function and Halo Bias on Precision Cosmology*, ApJ **713** (Apr., 2010) 856–864, [arXiv:0910.3668].

[26] C. E. Cunha and A. E. Evrard, *Sensitivity of galaxy cluster dark energy constraints to halo modeling uncertainties*, Phys. Rev. D **81** (Apr., 2010) 083509–+, [arXiv:0908.0526].

[27] P. S. Behroozi, R. H. Wechsler, and C. Conroy, *The Average Star Formation Histories of Galaxies in Dark Matter Halos from z=0-8*, *ArXiv e-prints* (July, 2012) [arXiv:1207.6105].

[28] J. Tinker, A. V. Kravtsov, A. Klypin, K. Abazajian, M. Warren, G. Yepes, S. Gottlöber, and D. E. Holz, *Toward a Halo Mass Function for Precision Cosmology: The Limits of Universality*, ApJ **688** (Dec., 2008) 709–728, [arXiv:0803.2706].

[29] M. S. Warren, K. Abazajian, D. E. Holz, and L. Teodoro, *Precision Determination of the Mass Function of Dark Matter Halos*, ApJ **646** (Aug., 2006) 881–885, [astro-ph/0506395].

[30] A. E. Evrard, T. J. MacFarland, H. M. P. Couchman, J. M. Colberg, N. Yoshida, S. D. M. White, A. Jenkins, C. S. Frenk, F. R. Pearce, J. A. Peacock, and P. A. Thomas, *Galaxy Clusters in Hubble Volume Simulations: Cosmological Constraints from Sky Survey Populations*, ApJ **573** (July, 2002) 7–36, [astro-ph/0110246].

[31] A. Jenkins et al., *The mass function of dark matter haloes*, MNRAS **321** (Feb., 2001) 372–384.

[32] R. Stanek, D. Rudd, and A. E. Evrard, *The effect of gas physics on the halo mass function*, MNRAS **394** (Mar., 2009) L11–L15, [arXiv:0809.2805].

[33] D. H. Rudd, A. R. Zentner, and A. V. Kravtsov, *Effects of Baryons and Dissipation on the Matter Power Spectrum*, ApJ **672** (Jan., 2008) 19–32, [astro-ph/0703741].

[34] D. Keres, M. Vogelsberger, D. Sijacki, V. Springel, and L. Hernquist, *Moving mesh cosmology: characteristics of galaxies and haloes*, *arXiv:1109.4638* (Sept., 2011) [arXiv:1109.4638].

[35] A. Simionescu, S. W. Allen, A. Mantz, N. Werner, Y. Takei, R. G. Morris, A. C. Fabian, J. S. Sanders, P. E. J. Nulsen, M. R. George, and G. B. Taylor, *Baryons at the Edge of the X-ray-Brightest Galaxy Cluster*, *Science* **331** (Mar., 2011) 1576–, [arXiv:1102.2429].

[36] K. Sharon, A. Gal-Yam, D. Maoz, A. V. Filippenko, R. J. Foley, J. M. Silverman, H. Ebeling, C.-J. Ma, E. O. Ofek, J.-P. Kneib, M. Donahue, R. S. Ellis, W. L. Freedman, R. P. Kirshner, J. S. Mulchaey, V. L. Sarajedini, and G. M. Voit, *The Type Ia Supernova Rate in Redshift 0.5-0.9 Galaxy Clusters*, ApJ **718** (Aug., 2010) 876–893, [arXiv:1006.3757].

[37] D. J. Sand, M. L. Graham, C. Bildfell, R. J. Foley, C. Pritchet, D. Zaritsky, H. Hoekstra, D. W. Just, S. Herbert-Fort, and S. Sivanandam, *Intracluster Supernovae in the Multi-epoch Nearby Cluster Survey*, ApJ **729** (Mar., 2011) 142, [arXiv:1011.1310].

[38] K. Barbary, G. Aldering, R. Amanullah, M. Brodwin, N. Connolly, K. S. Dawson, M. Doi, P. Eisenhardt, L. Faccioli, V. Fadeyev, H. K. Fakhouri, A. S. Fruchter, D. G. Gilbank, M. D. Gladders, G. Goldhaber, A. Goobar, T. Hattori, E. Hsiao, X. Huang, Y. Ihara, N. Kashikawa, B. Koester, K. Konishi, M. Kowalski, C. Lidman, L. Lubin, J. Meyers, T. Morokuma, T. Oda, N. Panagia, S. Perlmutter, M. Postman, P. Ripoche, P. Rosati, D. Rubin, D. J. Schlegel, A. L. Spadafora, S. A. Stanford, M. Strovink, N. Suzuki, N. Takanashi, K. Tokita, N. Yasuda, and Supernova Cosmology Project, *The Hubble Space Telescope Cluster Supernova Survey. II. The Type Ia Supernova Rate in High-redshift Galaxy Clusters*, ApJ **745** (Jan., 2012) 32, [arXiv:1010.5786].

[39] A. Gal-Yam, D. Maoz, P. Guhathakurta, and A. V. Filippenko, *A Population of Intergalactic Supernovae in Galaxy Clusters*, AJ **125** (Mar., 2003) 1087–1094, [astro-ph/0211334].

[40] P. Monaco, G. Murante, S. Borgani, and F. Fontanot, *Diffuse Stellar Component in Galaxy Clusters and the Evolution of the Most Massive Galaxies at z< ˜1*, ApJ **652** (Dec., 2006) L89–L92, [astro-ph/0610045].

[41] G. Murante, M. Giovalli, O. Gerhard, M. Arnaboldi, S. Borgani, and K. Dolag, *The importance of mergers for the origin of intracluster stars in cosmological simulations of galaxy clusters*, MNRAS **377** (May, 2007) 2–16, [astro-ph/0701925].

[42] M. Teyssier, K. V. Johnston, and M. M. Shara, *Wandering Stars: An Origin of Escaped Populations*, ApJ **707** (Dec., 2009) L22–L26, [arXiv:0911.0927].

[43] R. Napiwotzki and M. D. V. Silva, *Runaway and hypervelocity stars. The supernova connection*, *MmSAI* **83** (2012) 272, [arXiv:1109.4116].

[44] A. Klypin, S. Gottlöber, A. V. Kravtsov, and A. M. Khokhlov, *Galaxies in N-Body Simulations: Overcoming the Overmerging Problem*, ApJ **516** (May, 1999) 530–551.

[45] V. Springel, S. D. M. White, G. Tormen, and G. Kauffmann, *Populating a cluster of galaxies - I. Results at [formmu2]z=0*, MNRAS **328** (Dec., 2001) 726–750, [astro-ph/0012055].

[46] S. R. Knollmann and A. Knebe, *AHF: Amiga's Halo Finder*, ApJS **182** (June, 2009) 608–624, [arXiv:0904.3662].

[47] S. Planelles and V. Quilis, *ASOHF: a new adaptive spherical overdensity halo finder*, A&A **519** (Sept., 2010) A94, [arXiv:1006.3205].

[48] D. Tweed, J. Devriendt, J. Blaizot, S. Colombi, and A. Slyz, *Building merger trees from cosmological N-body simulations. Towards improving galaxy formation models using subhaloes*, A&A **506** (Nov., 2009) 647–660, [arXiv:0902.0679].

[49] A. Knebe, S. R. Knollmann, S. I. Muldrew, F. R. Pearce, M. A. Aragon-Calvo, Y. Ascasibar, P. S. Behroozi, D. Ceverino, S. Colombi, J. Diemand, K. Dolag, B. L. Falck, P. Fasel, J. Gardner, S. Gottlöber, C.-H. Hsu, F. Iannuzzi, A. Klypin, Z. Lukić, M. Maciejewski, C. McBride, M. C. Neyrinck, S. Planelles, D. Potter, V. Quilis, Y. Rasera, J. I. Read, P. M. Ricker, F. Roy, V. Springel, J. Stadel, G. Stinson, P. M. Sutter, V. Turchaninov, D. Tweed, G. Yepes, and M. Zemp, *Haloes gone MAD: The Halo-Finder Comparison Project*, MNRAS **415** (Aug., 2011) 2293–2318, [arXiv:1104.0949].

[50] E. Komatsu, K. M. Smith, J. Dunkley, C. L. Bennett, B. Gold, G. Hinshaw, N. Jarosik, D. Larson, M. R. Nolta, L. Page, D. N. Spergel, M. Halpern, R. S. Hill, A. Kogut, M. Limon,

S. S. Meyer, N. Odegard, G. S. Tucker, J. L. Weiland, E. Wollack, and E. L. Wright, *Seven-year Wilkinson Microwave Anisotropy Probe (WMAP) Observations: Cosmological Interpretation*, ApJS **192** (Feb., 2011) 18–+, [arXiv:1001.4538].

[51] V. Springel, *The cosmological simulation code GADGET-2*, MNRAS **364** (Dec., 2005) 1105–1134, [astro-ph/0505010].

[52] P. S. Behroozi, R. H. Wechsler, H.-Y. Wu, M. T. Busha, A. A. Klypin, and J. R. Primack, *Gravitationally Consistent Halo Catalogs and Merger Trees for Precision Cosmology*, *arXiv:1110.4370* (Oct., 2011) [arXiv:1110.4370].

[53] M. Trenti, B. D. Smith, E. J. Hallman, S. W. Skillman, and J. M. Shull, *How Well do Cosmological Simulations Reproduce Individual Halo Properties?*, ApJ **711** (Mar., 2010) 1198–1207, [arXiv:1001.5037].

[54] G. L. Bryan and M. L. Norman, *Statistical Properties of X-Ray Clusters: Analytic and Numerical Comparisons*, ApJ **495** (Mar., 1998) 80–+, [astro-ph/9710107].

[55] J. Barnes and P. Hut, *A hierarchical O(N log N) force-calculation algorithm*, Nature **324** (Dec., 1986) 446–449.

[56] J. F. Navarro, C. S. Frenk, and S. D. M. White, *A Universal Density Profile from Hierarchical Clustering*, ApJ **490** (Dec., 1997) 493–+, [astro-ph/9611107].

[57] D. Anderhalden and J. Diemand, *The total mass of dark matter haloes*, MNRAS **414** (July, 2011) 3166–3172, [arXiv:1102.5736].

[58] I. Ribas, C. Jordi, F. Vilardell, E. L. Fitzpatrick, R. W. Hilditch, and E. F. Guinan, *First Determination of the Distance and Fundamental Properties of an Eclipsing Binary in the Andromeda Galaxy*, ApJ **635** (Dec., 2005) L37–L40, [astro-ph/].

[59] R. Nandra, A. N. Lasenby, and M. P. Hobson, *The effect of a massive object on an expanding universe*, MNRAS **422** (June, 2012) 2931–2944, [arXiv:1104.4447].

[60] A. Loeb, *Cosmology with hypervelocity stars*, J. Cosmology Astropart. Phys. **4** (Apr., 2011) 23, [arXiv:1102.0007].

[61] M. T. Busha, F. C. Adams, R. H. Wechsler, and A. E. Evrard, *Future Evolution of Cosmic Structure in an Accelerating Universe*, ApJ **596** (Oct., 2003) 713–724, [astro-ph/0305211].

[62] M. T. Busha, A. E. Evrard, F. C. Adams, and R. H. Wechsler, *The ultimate halo mass in a ΛCDM universe*, MNRAS **363** (Oct., 2005) L11–L15, [astro-ph/0412161].

[63] F. Prada, A. A. Klypin, A. J. Cuesta, J. E. Betancort-Rijo, and J. Primack, *Halo concentrations in the standard Λ cold dark matter cosmology*, MNRAS **423** (July, 2012) 3018–3030, [arXiv:1104.5130].

[64] R. H. Wechsler, J. S. Bullock, J. R. Primack, A. V. Kravtsov, and A. Dekel, *Concentrations of Dark Halos from Their Assembly Histories*, ApJ **568** (Mar., 2002) 52–70, [astro-ph/0108151].

[65] S. W. Allen, D. A. Rapetti, R. W. Schmidt, H. Ebeling, R. G. Morris, and A. C. Fabian, *Improved constraints on dark energy from Chandra X-ray observations of the largest relaxed galaxy clusters*, MNRAS **383** (Jan., 2008) 879–896, [arXiv:0706.0033].